The type VII secretion system protects *Staphylococcus aureus* against antimicrobial host fatty acids

Arnaud Kengmo Tchoupa[1], Kate E. Watkins[1], Rebekah A. Jones[1], Agnès Kuroki[2], Mohammad Tauqeer Alam[1], Sebastien Perrier[1,2,3], Yin Chen[4], Meera Unnikrishnan[1*]

[1]Warwick Medical School, University of Warwick, Coventry, United Kingdom

[2]Department of Chemistry, University of Warwick, Coventry, United Kingdom

[3]Faculty of Pharmacy and Pharmaceutical Sciences, Monash University, Parkville, Victoria 3052, Australia

[4]School of Life Sciences, University of Warwick, Coventry, United Kingdom

Running title: *S. aureus* T7SS and fatty acid toxicity

[*]Corresponding author

Email: M.Unnikrishnan@warwick.ac.uk.

Summary

The *Staphylococcus aureus* type VII secretion system (T7SS) exports several proteins that are pivotal for bacterial virulence. The mechanisms underlying T7SS-mediated staphylococcal survival during infection nevertheless remain unclear. Here we show that the absence of EsxC, a small secreted effector implicated in bacterial persistence, results in cell membrane defects in *S. aureus*. Interestingly, isogenic mutants lacking EsxC, other T7SS effectors EsxA and EsxB, or the membrane-bound ATPase EssC, are more sensitive to killing by the host-derived antimicrobial fatty acid, linoleic acid (LA), compared to the wild-type (WT). LA induces more cell membrane damage in the T7SS mutants compared to the WT. Although WT and mutant strains did not differ in their ability to bind labelled LA, membrane lipid profiles show that T7SS mutants are less able to incorporate LA into their membrane phospholipids. Furthermore, proteomic analyses of WT and mutant cell fractions reveal that, in addition to compromising membranes, T7SS defects induce oxidative stress and hamper their response to LA challenge. Thus, our findings indicate that T7SS is crucial for *S. aureus* membrane integrity and homeostasis, which is critical when bacteria encounter antimicrobial fatty acids.

Keywords: *Staphylococcus aureus*, Type VII secretion system, long-chain unsaturated free fatty acids.

Introduction

Staphylococcus aureus is a facultative pathogen that can colonize the skin and nares of healthy individuals. The asymptomatic carriage of *S. aureus* is a major risk for subsequent infections (von Eiff *et al.*, 2001). *S. aureus* infections, which can be healthcare or community-associated, range from benign impetigo to life-threatening bacteraemia (Tong *et al.*, 2015). Clinical management of staphylococcal infections is complicated by the increasing prevalence of multidrug resistant strains (Lee *et al.*, 2018).

The success of *S. aureus* as a deadly pathogen is attributed to an array of virulence factors that facilitate host tissue adhesion and immune response evasion (Gordon & Lowy, 2008). One of these virulence factors is the type VII secretion system (T7SS), also known as the ESAT-6 secretion system (ESS). The orthologous ESX-1 system was initially discovered in *Mycobacterium tuberculosis*, where it is essential for bacterial virulence (Conrad *et al.*, 2017). T7SSs (T7SSb) are found in both Gram-positive and Gram-negative bacteria, although these systems and their secretion machineries appear to be distinct to their mycobacterial counterparts (Unnikrishnan *et al.*, 2017).

In extensively studied strains (COL, RN6390, USA300 and Newman), the T7SS consists of four integral membrane proteins (EsaA, EssA, EssB and EssC), two cytosolic proteins (EsaB and EsaG), five secreted substrates (EsxA, EsxB, EsxC, EsxD and EsaD), and EsaE, which interacts with the T7SS substrates to target them to the secretion apparatus (Cao *et al.*, 2016). A peptidoglycan hydrolase, EssH, was reported to mediate T7SS transport across the bacterial cell wall envelope (Bobrovskyy *et al.*, 2018).

The molecular architecture of the staphylococcal T7SS has not yet been fully characterized. T7SS integral membrane proteins EsaA, EssA, EssB, and EssC are thought to be the core of the T7 secretion machinery, with EssC being the central membrane transporter (Burts *et al.*, 2005, Jager *et al.*, 2018, Zoltner *et al.*, 2016). Interactions between secreted substrates and co-dependent secretion of substrates have been demonstrated (Anderson *et al.*, 2013, Cao *et al.*, 2016, Kneuper *et al.*, 2014, Ohr *et al.*, 2017). A recent study showed that the functional assembly of the T7SS machinery in *S. aureus* is supported by the flotillin homolog FloA, within functional membrane microdomains (Mielich-Suss *et al.*, 2017).

The *S. aureus* T7SS is pivotal for bacterial virulence. Indeed, S. *aureus* mutants lacking the entire T7SS (Kneuper *et al.*, 2014) or specific T7SS components (EsxA, EssB, EssC, EsxC, EsxB, EsaB, EsaD or EsaE) were consistently shown to be less virulent and/or persistent in various mouse infection models (Anderson *et al.*, 2011, Anderson *et al.*, 2017, Burts *et al.*, 2008, Burts *et al.*, 2005, Ishii *et al.*, 2014, Lopez *et al.*, 2017). EsxA is necessary to delay apoptosis of *S. aureus*-infected epithelial and dendritic cells, while other substrates modulate cytokine production (Anderson *et al.*, 2017, Cruciani *et al.*, 2017, Korea *et al.*, 2014). Although the relevance of T7SS to *S. aureus* is less understood, a role for the toxin-antitoxin pair EsaD (or EssD) and EsaG (or EssI) was recently demonstrated in intraspecies competition (Cao *et al.*, 2016, Ohr *et al.*, 2017).

Interestingly, *S. aureus* T7SS expression is induced in response to host-specific FAs (Ishii *et al.*, 2014, Kenny *et al.*, 2009, Lopez *et al.*, 2017), although the role of T7SS in bacterial resistance to antimicrobial FAs remains unclear. In this study, we demonstrate that *S. aureus* lacking the T7SS substrate EsxC has a defective cell membrane. Intriguingly, EsxC and other T7SS mutants were more sensitive to an

unsaturated FA, linoleic acid (LA), compared to the wild-type (WT). Although there were no differences in binding labelled LA, LA induced a more leaky membrane in the T7SS mutants, and there was less incorporation of LA into membrane phospholipids. Cellular proteomics revealed that in addition to membrane discrepancies, T7SS mutants exhibited different redox and metabolic states, which likely result in a distinct response to LA.

Results

The type VII substrate EsxC is present on the staphylococcal surface and affects its composition

EsxC, a small 15-kDa protein secreted by the T7SS, is important for *S. aureus* persistence in mice (Burts *et al.*, 2008). However, mechanisms underlying EsxC- or T7SS-mediated bacterial survival are not known. In order to understand the role of EsxC, we generated an isogenic *esxC* mutant as described previously (Bae & Schneewind, 2006), and confirmed the absence of any secondary site mutations by whole genome sequencing. Δ*esxC* had a similar growth rate to the WT USA300 JE2 strain (Fig. S1). EsxC is known to be a secreted effector of T7SS (Burts *et al.*, 2008), although it has been consistently detected in cell membrane (CM) fractions of RN6390 and USA300 (Bobrovskyy *et al.*, 2018, Kneuper *et al.*, 2014). As reported previously, we detected EsxC in the CM fractions of the WT but not in Δ*esxC* (Fig. S2). Moreover, we also detected EsxC in the WT cell wall (CW) fraction (Fig. S2). In a deletion mutant of the membrane-bound major ATPase EssC (a core T7SS component), EsxC was detected in CM and CW preparations even in the absence of EssC (Fig. S2). While we were unable to detect EsxC in the cell-free supernatants by immunoblotting, we

detected this protein by secretome analyses. Along with EsxC, other T7SS proteins, EsxA and EsxD, were detected in the WT but not in Δ*esxC or* Δ*essC* supernatants (Table S1).

Given the association of EsxC with the cell membrane, we stained the WT, Δ*esxC* and Δ*essC* mutants with FM-143, a fluorescent cell membrane probe (Pulschen *et al.*, 2017). We observed a mild but statistically significant increase in FM-143 staining in the mutants as compared to the WT (Fig. 1A). Increased staining of membranes by FM-143 has been associated previously with membrane blebbing in bacteria (Wood *et al.*, 2019).

To study if the lack of T7SS proteins affected other surface proteins, a surface proteome analysis of the WT and mutants was carried out using trypsin treatment to digest surface proteins (Solis *et al.*, 2014). We found that most proteins (172/218) were less abundant in Δ*esxC* compared to the WT (Fig. S3). Interestingly, majority of relatively less abundant proteins (16/20) in the Δ*esxC* surface proteome were predicted or proven to be cytosolic (Table S2). Metabolic (PfKA, FolD, FabI GatB, and ImdH) or stress-related (Asp23 and putative universal stress proteins) proteins were lowest in abundance ($\log_2$ fold change < - 1.0). The T7SS core component EsaA, which has a prominent extracellular loop (Dreisbach *et al.*, 2010), was also ~50% less abundant in Δ*esxC*, implying that EsxC absence may affect T7SS assembly. Identification of cytosolic proteins during surface proteome analysis could be attributed to non-canonical secretion of cytosolic proteins that bind to bacterial surfaces (Hempel *et al.*, 2011, Pasztor *et al.*, 2010) or cell lysis during sample preparation (Dreisbach *et al.*, 2010, Solis *et al.*, 2014, Ventura *et al.*, 2010). To study if the T7SS mutants were more resistant to cell lysis, we compared the Triton X-100 lysis of WT, Δ*esxC* and,

138 Δ*essC* in PBS in non-growing conditions. While Δ*esxC* was slightly more resistant to
139 Triton X-100, Δ*essC* was clearly defective in lysis (Fig. 1B), as compared to the WT.

140 We probed T7SS effects on the membrane further by assessing membrane fluidity of
141 the WT and Δ*esxC* mutant. We used pyrene decanoic acid, an eximer-forming lipid
142 (Lopez *et al.*, 2017), to measure the fluidity of WT and Δ*esxC* membranes. Compared
143 to the WT, the cytosolic membrane of the Δ*esxC* mutant showed a mild but statistically
144 significant increase in rigidity (Fig. 1C). Furthermore, we stained WT and with a
145 fluorescent membrane dye DiI12C, which has been used detect regions of increased
146 fluidity in bacteria (Saeloh *et al.*, 2018). As reported previously for *S. aureus*, we
147 observe few fluid regions in the WT, and an uneven staining of the membrane. In
148 contrast, a very weak staining of the membranes was observed for the Δ*esxC* mutant,
149 (Fig 1 D and E), which may indicate a decrease in membrane fluidity.

150 Overall, the data indicate that EsxC contributes to *S. aureus* cell surface structure and
151 membrane fluidity.

152

153 **_S. aureus esxC_ and _essC_ mutants are more sensitive to antimicrobial fatty acids**

154 Multiple studies have reported the activation of the T7SS, when *S. aureus* is grown in
155 presence of host FAs (Ishii *et al.*, 2014, Kenny *et al.*, 2009, Lopez *et al.*, 2017). Given
156 our findings that the *esxC* mutant has membrane defects and that the *esxC* deletion
157 affects the surface abundance of IsdA, which is essential for *S. aureus* resistance to
158 antimicrobial fatty acids (Clarke *et al.*, 2007), we cultured WT USA300 and its isogenic
159 *essC* or *esxC* mutant in the presence of an unsaturated FA (C18:2), linoleic acid (LA),
160 at a concentration (80 μM) that still allows WT growth. Bacteria were also cultured in
161 parallel in presence of stearic acid (SA), a saturated C18:0 FA. The T7SS mutants

displayed impaired growth in presence of LA but not SA, as measured by optical density (OD) (Fig. 2A) or colony forming units (CFU) (Fig. 2B). Importantly, Δ*esxC* complemented with a plasmid containing the *esxC* gene reverted to the WT phenotype (Fig. 2C). The increased susceptibility of T7SS mutants to antimicrobial fatty acids was not restricted to linoleic acid; when cultured in the presence of arachidonic acid, another unsaturated FA (C20:4), growth of Δ*esxC* and Δ*essC* were inhibited more as compared to the WT (Fig. S4)

T7SS substrates contribute to *S. aureus* resistance to LA toxicity

Next, we investigated whether T7SS proteins other than *essC* and *esxC* contributed to *S. aureus* growth in presence of LA. Mutants lacking two other substrates, Δ*esxA* and Δ*esxB*, were grown in presence of FAs. Both mutants grew slower than the WT USA300 (Fig. S5A). To ensure that the increased sensitivity observed for the T7SS mutants was not strain specific, RN6390 Δ*essC* or Δ*esxC* and Newman Δ*esxA* or Δ*esxB* mutants were tested. Similar to the USA300 mutants, the growth of all these T7SS mutants was also impacted in the presence of LA (Fig. S5B and C). The growth defect in Newman Δ*esxA* was abrogated upon complementation (Fig. 2D). Of note, the Newman WT was readily inhibited by a lower concentration of LA (40 μM), which is in agreement with the lower T7SS expression levels in this strain compared to USA300 (Anderson *et al.*, 2013, Kneuper *et al.*, 2014). We conclude that a functional T7SS plays a role in *S. aureus* resistance to LA toxicity.

T7SS is required for maintaining membrane integrity in presence of LA

185 To study the mechanisms involved in T7SS mediated protection to LA toxicity, further
186 studies were performed using strains lacking esxC, a representative T7SS effector, or
187 essC the main T7SS transporter. As our membrane and surface proteome analyses
188 with Δ*esxC* suggested that the bacterial envelope is altered upon T7SS defect, we
189 wanted to test if LA-mediated growth inhibition was due to an increased binding of LA
190 to T7SS mutants. To do this, we chemically engineered LA to produce an azide
191 functionalised LA (N^6-diazo-N^2-((9Z,12Z)-octadeca-9,12-dienoyl)lysine, N_3-LA) or
192 azide-LA (Fig. 3A). After incubating bacteria with azide-LA, click-chemistry with an
193 alkyne dye (Click-iT™ Alexa Fluor™ 488 sDIBO alkyne) was used to stain azide-LA
194 associated with bacteria. There were no obvious differences in the fluorescence from
195 Δ*essC* and Δ*esxC* compared to the WT (Fig. 3B), suggesting that T7SS components
196 are not involved in binding or sequestering LA. However, when bacteria treated with
197 azide-LA were stained with propidium iodide (PI), a good indicator of membrane
198 integrity, Δ*essC* and Δ*esxC* displayed a more intense PI staining compared to the WT
199 (Fig. 3C and D). Similarly, when WT and mutants were stained with PI and SYTO 9
200 after treatment with 80 µM unlabelled LA, we observed an increased PI staining (Fig.
201 4A and B) and therefore lower SYTO 9 / PI (Live/Dead) ratio for both mutants (Figure
202 4C). These data suggest that an intact T7SS helps *S. aureus* to maintain its membrane
203 integrity when faced with the detergent-like effects of unsaturated FAs.

204

205 **LA-incorporation into membrane phospholipids is modulated by T7SS**

206 As the T7SS mutants have more compromised cell membranes in presence of LA, we
207 next investigated if membrane lipids were altered in the T7SS mutants. Lipids from
208 WT USA300 and T7SS mutants were analysed by high-performance liquid

chromatography (HPLC)-mass spectrometry (MS) in negative ionisation mode. As reported previously (Delekta *et al.*, 2018, Parsons *et al.*, 2011), phosphatidylglycerol (PG) was the major phospholipid present in the membrane of WT grown in TSB (Fig. S6A). Δ*essC* and Δ*esxC* grown with or without 10 μM LA [(a concentration that has been previously shown to be sub-inhibitory for USA300 (Lopez *et al.*, 2017)] displayed lipid profiles similar to that of WT (Fig. S6A and B). Notably, PG molecular species were significantly altered upon growth in LA-supplemented TSB for WT (Fig. 5A), Δ*essC* (Fig. S6C) and Δ*esxC* (Fig. 5B). Three new LA-specific PG species with mass to charge ratios (m/z) 731 (C33:2), 759 (C35:2), and 787 (C37:2) appeared to contain LA (C18:2) or its elongated C20:2 or C22:2 versions, as revealed by their fragmentations (Fig. S7A, B and C). PG species containing exogenous, unsaturated FAs were also present in Δ*essC* and Δ*esxC*. However, LA (C18:2)-containing PG species (C33:2) were less abundant in the *esxC* mutant compared to WT (Fig. 5C). A similar trend, although statistically non-significant ($P > 0.05$), was observed for C20:2- and C22:2-containing PG species (Fig. S7D and E), and when all the unsaturated exogenous PG species were combined (Fig. 5D). The data suggest that a T7SS defect may compromise the incorporation and elongation of LA in *S. aureus* membranes.

T7SS mutations affect the total cellular content and *S. aureus* responses to LA

In order to gain further insight into T7SS-mediated modulation of proteins involved in FA incorporation and membrane homeostasis in presence of LA, we used an unbiased proteomic approach to study protein profiles of WT USA300, Δ*essC*, and Δ*esxC* grown exponentially with or without 10 μM LA. Of note, WT and both these T7SS mutants grew similarly in presence of up to 40 μM LA (Fig. S8).

WT vs T7SS mutants in absence of LA treatment: Interestingly, Δ*essC* or Δ*esxC* cultured in TSB readily displayed proteins with changed abundance when compared to the WT, with 37 and 24 proteins significantly ($P < 0.05$) altered in Δ*essC* and Δ*esxC*, respectively. Similarly, 14 proteins were differentially abundant in both Δ*essC* and Δ*esxC* (Fig. 6A and B). These included proteins associated with signal transduction (LytR and ArlR), the CW (acetyltransferase GNAT, FnbB and MazF), DNA repair (MutL and RadA), nucleotide binding (ATP-grasp domain protein and YqeH), hydrolysis (amidohydrolase), cell stress response [universal stress protein (Usp) family], or were uncharacterised (A0A0H2XGJ8, YbbR and lipoprotein) (Fig. 6B and Table 1). Of the 33 proteins changed only in Δ*essC* (23 proteins) or Δ*esxC* (10 proteins), nearly 40% (13 proteins) were associated with oxidation-reduction and other metabolic processes. Ten membrane proteins were more abundant in Δ*essC* (Table 1), which included SrrB, a membrane protein that is activated by impaired respiration (Mashruwala *et al.*, 2017), and whose gene expression increased 6 times upon growth in presence of LA (Lopez *et al.*, 2017). SrrB was also detected at higher levels in the *esxC* mutant although the increase was non-significant ($P = 0.07$).

Table 1. Proteins with changed abundance in Δ*essC* and Δ*esxC* mutants relative to the WT USA300 JE2

		Δ*essC*/WT		Δ*esxC*/WT		
Functions	**Uniprot ID**	**Log_2 FC**	**Adjusted *P* value**	**Log_2 FC**	**Adjusted *P* value**	**Description**
Signal transduction systems	Q2FK09	-3.0	4.90E-13	-3.1	4.90E-13	Sensory transduction protein LytR
	Q2FH23	-2.9	0.002527	-2.1	0.026184	Response regulator ArlR
Membrane proteins	A0A0H2XF42	3.0	1.75E-10	0	1	Cytochrome D ubiquinol oxidase, subunit I
	A0A0H2XDZ5	1.7	1.68E-05	0	1	Uncharacterized membrane protein
	A0A0H2XFJ8	2.0	0.001077	0.5	0.883953	Uracil permease
	A0A0H2XGW7	2.7	0.005757	2.5	0.010784	Putative lipoprotein
	A0A0H2XIA9	1.0	0.006115	0	1	Protein translocase subunit SecY
	Q2FIN2	1.6	0.029451	0.5	0.970614	Prolipoprotein diacylglyceryl transferase LGT
	A0A0H2XKD9	2.0	0.038093	1.8	0.070347	Staphylococcal respiratory response protein SrrB
	A0A0H2XFE1	3.4	0.039814	1.1	0.970614	Peptidase
	A0A0H2XJV8	2.0	0.04444	1.5	0.231285	Cyclic-di-AMP phosphodiesterase
	A0A0H2XGF4	3.0	0.044681	0.9	0.986458	Sodium:dicarboxylate symporter family protein
	A0A0H2XHV2	2.5	0.049168	2.4	0.070182	Glycine betaine transporter OpuD
Stress response	A0A0H2XKH6	2.2	5.80E-05	2.5	1.07E-05	Universal stress protein family
	A0A0H2XIZ0	0.0	1	-3.4	1. 06E-10	OsmC/Ohr family protein
DNA repair	Q2FHE2	-2.3	1.79E-08	-2.3	1.19E-08	DNA mismatch repair protein MutL
	A0A0H2XI63	-2.0	0.004036	-2.0	0.004036	DNA repair protein RadA
	A0A0H2XHT1	-0.3	0.708343	-1.9	0.008379	Formamidopyrimidine-DNA glycosylase MutM
Oxidation-reduction process	A0A0H2XJ90	1.1	0.038093	1.0	0.088334	D-isomer specific 2-hydroxyacid dehydrogenase family protein
	A0A0H2XHE0	2.4	0.039099	-0.1	1	Thiol-disulphide oxidoreductase, DCC family protein
	A0A0H2XGR9	0.0	1	1.4	8.89E-08	Oxidoreductase, Gfo/Idh/MocA family
	A0A0H2XK08	1.0	0.406975	2.9	0.00791	Oxidoreductase, short chain dehydrogenase/reductase family
	A0A0H2XFZ3	-0.8	0.404225	2.1	0.016405	Nitroreductase family protein
Hydrolases	A0A0H2XE49	2.9	1.07E-06	2.9	5.99E-07	Amidohydrolase
	Q2FES9	-2.7	0.003385	-0.3	1	Uncharacterized hydrolase
	A0A0H2XFF2	-0.8	0.016697	-0.5	0.157809	Peptidase, U32 family
	A0A0H2XJH8	0.0	1	2.8	1.06E-10	Peptidase M20 domain-containing protein 2
	A0A0H2XJ54	0.0	1	2.0	0.000949	Hydrolase (HAD superfamily)
	Q2FEG2	-0.2	0.854748	-2.9	0.004615	Formimidoylglutamase
Metabolism	A0A0H2XGU2	-1.6	4.99E-06	-0.1	1	Pseudouridine synthase
	A0A0H2XK15	2.8	0.004424	0.9	0.777138	1-phosphatidylinositol phosphodiesterase
	Q2FEK2	-1.6	0.038093	-0.3	1	Urease accessory protein UreE
	Q2FI05	1.1	0.038093	0.0	1	Bifunctional purine biosynthesis protein PurH
	Q2FIL2	2.9	0.038093	0.8	0.970614	SsrA-binding protein
	A0A0H2XII6	1.8	0.038093	1.5	0.088334	Orn/Lys/Arg decarboxylase
	A0A0H2XJR8	-0.9	0.04444	-0.5	0.61246	RNA methyltransferase, RsmD family
	A0A0H2XKG7	0.0	1	1.4	8.18E-08	Aspartokinase
Cell wall composition	A0A0H2XJQ4	-4.0	4.92E-11	-4.0	3.28E-11	Acetyltransferase, GNAT family
	A0A0H2XKG3	-2.3	0.001238	-1.7	0.016405	Fibronectin binding protein B
	A0A0H2XJC8	-2.3	0.009779	-3.0	0.000819	Phi77 ORF017-like protein (Toxin MazF)
	Q2FE03	0.0	1	2.6	1.18E-12	Fibronectin-binding protein A
Nucleotide binding	A0A0H2XHY5	-2.3	8.58E-06	-2.3	6.01E-06	ATP-grasp domain protein
	A0A0H2XFA5	3.3	0.014259	3.5	0.008379	Putative GTP-binding YqeH protein
Uncharacterised proteins	A0A0H2XGJ8	2.2	0.000372	2.4	9.41E-05	Uncharacterized protein
	A0A0H2XE09	2.1	0.008231	1.9	0.016405	Ybbr-like uncharacterized protein
	Q2FFI4	3.4	0.020136	0.9	0.970614	UPF0316 membrane protein
	A0A0H2XG24	1.1	0.022345	0.8	0.088334	Uncharacterized protein

WT vs T7SS mutants in presence of LA: We then compared the proteomic profiles of LA-treated strains (WT, Δ*essC* or Δ*esxC*) with their untreated counterparts. Clearly, the principal component analysis revealed that the differences due to the genetic makeup (WT or T7SS mutants) were less prominent than the dramatic changes induced by LA (Fig. S9). These changes are exemplified for the WT; 163/1132 proteins identified had an altered relative abundance upon growth with LA (Fig. 6C). 167 and 171 proteins were changed ($P < 0.05$) in Δ*essC* and Δ*esxC*, respectively, in response to LA, of which ~ 40% (68 proteins) were common to these mutants and their WT (Fig. 6D). At least 30% of the significantly changed proteins ($P < 0.05$) were unique to WT (53 proteins), Δ*essC* (50 proteins), or Δ*esxC* (64 proteins) (Fig. 6D), suggesting that each strain responds differently to LA. However, almost all proteins (13/14 proteins) that were similarly deregulated in Δ*essC* and Δ*esxC* grown without LA (Fig. 6B) were modulated in presence of LA (highlighted in bold in Dataset S1). Proteins that were less abundant in both mutants were, upon LA treatment, either increased to WT levels (MutL, acetyltransferase GNAT, Toxin MazF, and ATP-grasp domain protein), or were unchanged in the mutants and decreased in the LA-treated WT (LytR and FnbB) (Dataset S1). Likewise, proteins with increased amounts in Δ*essC* or Δ*esxC* were: (i) downregulated to WT levels in response to LA (putative lipoprotein A0A0H2XGW7), (ii) unaltered in both mutants and upregulated in WT (Usp, amidohydrolase, and YbbR), (iii) or further increased in the *essC* mutant and strongly upregulated in WT (A0A0H2XGJ8) (Dataset S1). In sum, except for ArlR and RadA that were conversely regulated in all strains after LA treatment, proteins similarly deregulated in Δ*esxC* and Δ*essC* were returned to similar levels in response to LA. A similar trend was observed for 15/23 and all 10 proteins exclusively more or less abundant in Δ*essC* and Δ*esxC*, respectively.

Altered molecular functions in presence of LA: We then used QuickGO (a web-based tool for Gene Ontology searching) (Binns *et al.*, 2009) to retrieve GO terms associated with the ten most significantly upregulated proteins in LA-treated WT (Dataset S1). Strikingly, 9/10 proteins had a hydrolase or an oxidoreductase activity. A comprehensive, statistical analysis showed a clear enrichment of 8 specific molecular functions ($P < 0.05$) in at least one strain (WT or T7SS mutants) (Fig. 7A). Oxidoreductase and hydrolase activities were enhanced in LA-treated WT, while Δ*essC* and Δ*esxC* were less able to upregulate proteins with these molecular functions. Flavin adenine dinucleotide (FAD)-binding, which plays a role in oxidation-reduction and FA metabolic processes, was similarly more enriched in the LA-treated WT. In contrast, transferase activity, which is linked to CW synthesis, was induced more in T7SS mutants compared to the WT. Molecular functions that are decreased upon LA challenge were also determined (Fig. 7B). In agreement with reduced intracellular ATP levels following membrane damage by antimicrobial FAs (Cartron *et al.*, 2014), genes with the ATP-binding function (mainly ATP-binding ABC transporters) were strongly inhibited in the WT. ATP-dependent lyases were also repressed in the WT. On the contrary, T7SS mutants were less able to modulate ATP-binding proteins. Instead, a strong inhibition of ribosomal constituents and other translation-related components was seen (Fig. 7B).

To test the oxidoreductive states of the WT and the mutants, we stained bacteria with dichlorofluorescin (DCF), which detects reactive oxygen species (George *et al.*, 2019). Reflecting the changes seen in the proteomics data, when treated with 10 μM LA there is an increase in the ROS generated in the T7SS mutants compared to the WT (Fig 7C). However, in bacteria grown without LA, the mutants have slightly less or no change in the ROS generated compared to WT (Figure 7D). Taken together, our

proteomic analyses reveal that the lack of T7SS induces altered membrane and metabolic states indicative of oxidative stress responses. While the WT shows a multifaceted response to mitigate LA-induced damage on the bacterial membrane, such responses are clearly altered in the absence of the T7SS.

Discussion

Host fatty acids (FAs) play a crucial role in the host defence to *S. aureus* infections. *S. aureus* is particularly sensitive to unsaturated FAs, which are abundant in the human skin (Clarke *et al.*, 2007, Parsons *et al.*, 2012, Arsic *et al.*, 2012, Kelsey *et al.*, 2006, Kenny *et al.*, 2009). We report here that the T7SS, an important component of *S. aureus* virulence arsenal, is critical in modulating the response to antimicrobial host FAs by maintaining the bacterial cell membrane integrity. Specifically, we demonstrate that a T7SS substrate, EsxC, impacts *S. aureus* membrane properties. A functional T7SS enables bacteria to mitigate LA-induced toxicity and grow better than mutants with a compromised T7SS. In the absence of T7SS components, LA is less incorporated into membrane phospholipids and enhances cell membrane damage, while bacteria are unable to activate adaptive mechanisms involved in LA resistance, as indicated by cellular proteomics.

Although several studies have shown multiple interactions between the staphylococcal T7SS components, the precise molecular architecture of this system remains unclear. EsxC (previously EsaC) was first described as a secreted protein (Burts *et al.*, 2008). However, in keeping with prior studies, we found that EsxC can also localize within staphylococcal membranes (Bobrovskyy *et al.*, 2018, Kneuper *et al.*, 2014). Based on available data, EsxC is likely to be associated to EsxA, EsaD, or EsaE on the

membrane (Anderson *et al.*, 2013, Anderson *et al.*, 2017, Cao *et al.*, 2016). Additionally, the reduced EsaA protein levels that we found on the surface of *S. aureus* USA300 Δ*esxC* combined with prior observations of diminished EsxC protein levels in RN6390 Δ*esaA* membranes (Kneuper *et al.*, 2014) suggest that EsxC may interact with EsaA, a key component of the T7SS core (Aly *et al.*, 2017), in *S. aureus* membranes.

T7SS integral membrane proteins interact with the flotillin homolog FloA within functional membrane microdomains (FMMs) (Mielich-Suss *et al.*, 2017). FMMs were recently shown to contain staphyloxanthin derivatives (Garcia-Fernandez *et al.*, 2017), which are known to increase membrane rigidity (Chamberlain *et al.*, 1991, Sen *et al.*, 2016, Tiwari *et al.*, 2018). Hence, well-structured FMMs may play a role in *S. aureus* membrane fluidity as reported for *Bacillus subtilis* (Bach & Bramkamp, 2013). Interestingly, mutations or treatments affecting *S. aureus* membrane fluidity also modulate T7SS transcription (Lopez *et al.*, 2017, Ishii *et al.*, 2014, Parsons *et al.*, 2014). Hence, there appears to be a link between membrane fluidity and T7SS in *S. aureus*. Also, the state of the membrane was suggested to trigger the production of T7SS (Lopez *et al.*, 2017). Remarkably, deletion of *esxC* led to a mild increase in bacterial membrane rigidity and membrane defects (Fig. 1), suggesting membrane modulation by the T7SS. Possibly, interactions between FloA and T7SS are perturbed upon *esxC* deletion and affect *S. aureus* FMMs. We surmise that a functional T7SS helps *S. aureus* to maintain its membrane architecture.

The current cellular proteomics data reveal that the abundance of more proteins is altered in Δ*essC* (37) than *esxC* (24) in comparison to *S. aureus* WT, which is in keeping with the greater importance of EssC as the conserved driving force of the T7SS (Warne *et al.*, 2016). Importantly, almost 60% of proteins deregulated in Δ*esxC*

are similarly affected in Δ*essC*, strongly suggesting that any modification of the T7SS core leads to a similar staphylococcal response. Surprisingly, proteins with altered abundance in USA300 Δ*essC* were distinct to the ferric uptake regulator (Fur)-controlled genes differentially expressed in RN6390 Δ*essC* (Casabona *et al.*, 2017b). This discrepancy might be due to strain differences, including *rsbU* defect in RN6390 that impairs SigB activity (Cassat *et al.*, 2006, Giachino *et al.*, 2001). Nevertheless, given the known role of Fur in oxidative stress resistance (Horsburgh *et al.*, 2001, Johnson *et al.*, 2011), both mutants may display an altered oxidative status following *essC* deletion. *S aureus* RN6390 also differentially expresses redox-sensitive genes in absence of EsaB (Casabona *et al.*, 2017a). Also, since the T7SS substrate EsxA is upregulated in response to hydrogen pyroxide (Casabona *et al.*, 2017b), one could speculate that lack of T7SS stimulates an oxidative stress response. A further indication of altered physiological states of Δ*essC* and Δ*esxC* was the decreased abundance of the two-component regulatory system proteins, LytSR, ArlSR and SrrAB, which was consistent with down-regulation of *lytR* transcription observed previously in the absence of *arlR* (Liang *et al.*, 2005). Importantly, the *S. aureus* response to antimicrobial FAs includes downregulation of *lytRS* (Kenny *et al.*, 2009, Neumann *et al.*, 2015), and upregulation of *srrB* (Lopez *et al.*, 2017). Given that LytSR is involved in bacterial surface and membrane potential modulation (Patton *et al.*, 2006, Groicher *et al.*, 2000), T7SS defects are likely to result in an altered cell envelope.

It is striking that the staphylococcal T7SS is strongly upregulated in presence of sub-inhibitory concentrations of LA (Kenny *et al.*, 2009, Lopez *et al.*, 2017). FAs with more cis double bonds, which are more toxic toward *S. aureus* (Parsons *et al.*, 2012), are also more potent T7SS activators (Lopez *et al.*, 2017). Our current study interestingly

suggests a protective role of T7SS against LA toxicity. Previously described *S. aureus* antimicrobial FA (AFA) resistance mechanisms, including IsdA or wall teichoic acid-mediated modulation of cellular hydrophobicity (Clarke *et al.*, 2007, Kohler *et al.*, 2009, Parsons *et al.*, 2012, Moran *et al.*, 2017), and AFA detoxification with the efflux pumps Tet38 and FarE (Alnaseri *et al.*, 2015, Truong-Bolduc *et al.*, 2014), do not appear to explain the increased susceptibility of T7SS mutants to LA, as indicated by cellular proteomics. In line with a role for T7SS in the oxidative stress response, T7SS mutants were less able to prime their redox-active proteins in response to LA-induced oxidative stress. Instead, to cope with LA, they appear to rely on strong inhibition of the protein synthesis machinery, which is reminiscent of the stringent response (Geiger *et al.*, 2012).

The Fak pathway which is required for incorporation of exogenous FA into membrane phospholipids via a two-component fatty acid kinase (Fak) (Nguyen *et al.*, 2016, Parsons *et al.*, 2012, Parsons *et al.*, 2014), was reported to be important for T7SS activation by unsaturated FA (Lopez *et al.*, 2017). FakB1 and FakB2, bind to FAs, and FakB-bound FAs are phosphorylated by FakA prior to their incorporation (Parsons *et al.*, 2014). In presence of inhibitory concentrations of unsaturated FA like LA, while FA is incorporated into the membrane lipids, free LA causes pore formation that leads to bacterial lysis (Greenway & Dyke, 1979). Our lipidomic analyses revealed that in the absence of T7SS, bacteria were less able to incorporate LA into their phospholipids (Figure 5), and displayed an increased membrane permeability in presence of LA. However, it seems counterintuitive that LA incorporation was impacted more in Δ*esxC* than in Δ*essC* given the central role of EssC in T7 secretion (Burts *et al.*, 2005, Jager *et al.*, 2018, Zoltner *et al.*, 2016). It is possible that EsxC that accumulates in the membrane (Fig. 1A) in the absence of protein secretion by the main transporter, EssC,

mediates partial LA incorporation in the *essC* mutant; secretion per se may not be required for LA incorporation. It is also worth noting that transcript levels of *esxC*, and not *essC*, were strongly upregulated in a *S. aureus fakA* mutant (Parsons *et al.*, 2014). As protein levels of Fak proteins in the T7SS mutants stay unaltered in presence or absence of LA, suggesting no T7SS-mediated regulatory control of the Fak pathway, we speculate that EsxC and other interdependent T7SS substrates play an important role in facilitating Fak function in *S. aureus* membranes, either by mediating recruitment or targeting of Fak proteins to the membrane. Our findings warrant further investigations into molecular mechanisms underlying T7SS-mediated FA incorporation within staphylococcal membranes.

The increased susceptibility of T7SS mutants to LA might explain why they are less virulent in environments rich in LA and other AFAs like the mouse lungs (Δ*essC*) (Ishii *et al.*, 2014), abscesses (Δ*esxC* and Δ*esaB*), liver and skin (Δ*essB*) (Wang *et al.*, 2016, Lopez *et al.*, 2017). Previous research showing T7SS induction by host-derived FAs further supports the importance of T7SS in such environments (Lopez *et al.*, 2017, Ishii *et al.*, 2014). Taken together, we conclude that T7SS plays a key role in modulating the *S. aureus* cell membrane in response to toxic host FAs. Although, at present, it is unclear how T7SS contributes to staphylococcal membrane architecture, T7SS interaction with the flotillin homolog FloA within functional membrane microdomains (Mielich-Suss *et al.*, 2017) corroborates the idea that T7SS proteins interact with many other proteins to modulate *S. aureus* membranes. Indeed, our data also suggest that blocking T7SS activity would make *S. aureus* more vulnerable to AFAs, a key anti-staphylococcal host defence, thus making T7SS a very attractive drug target.

Experimental procedures:

Bacterial strains and growth conditions. *S. aureus* strains used are listed in Table S3, and were grown aerobically in tryptic soy broth (TSB) overnight (O/N) at 37ºC for each experiment unless stated otherwise. For complemented *S. aureus* strains, TSB was supplemented with 10 µg/mL chloramphenicol.

Construction of bacterial mutants. The primers used are listed in Table S4. In-frame deletion of *essC* or *esxC* was performed as described previously (Bae & Schneewind, 2006). Briefly, 1-kb DNA fragments up and downstream of the targeted gene sequence were PCR-amplified from USA300 LAC JE2 chromosomal DNA, and both PCR products fused via SOEing (splicing by overlap extension)-PCR. The 2-kb DNA fragment obtained was cloned into pKORI, and used for in-frame deletion. Putative mutants were screened by PCR-amplification of a fragment including the gene of interest, whose deletion was confirmed by Sanger sequencing. Further, to confirm that successful mutants did not have any additional mutations, Illumina whole genome sequencing was performed on libraries prepared with the Nextera XT kit and an Illumina MiSeq® instrument following manufacturers' recommendations. For complementation, full-length *esxC* gene was cloned onto pOS1CK described previously (Korea *et al.*, 2014).

Membrane fluidity assay. O/N bacterial cultures were diluted to an OD_{600} of 0.15 in TSB, and were grown to an OD_{600} of 1 (OD1). Bacteria were washed with PBS prior to treatment for 30 min at 37ºC with 37.5 µg/mL lysostaphin in PBS containing 20% sucrose. The spheroblasts were then centrifuged at 8000 × *g* for 10 min, and the pellet resuspended in the labelling solution (PBS, 20% sucrose, 0.01% F-127, 5 µM pyrene decanoic acid). The incubation in the dark was done for 1h at 25ºC under gentle rotation. PBS supplemented with 20% sucrose was used to wash the stained

449 spheroblasts that were afterwards transferred to 96-well plates for fluorescence
450 measurements as previously described (Lopez *et al.*, 2017).

451 **Triton X-100 lysis assays.** Whole cell autolysis assays were performed as described
452 elsewhere with a few modifications (Mashruwala *et al.*, 2017). Specifically, OD1-grown
453 *S. aureus* USA300 JE2 WT, *essC* and *esxC* mutants were extensively washed with
454 PBS followed by ice-cold water, and resuspended in PBS with 0.1% Triton X-100 to
455 an OD_{600} of 0.7. Subsequently, the samples were incubated with shaking at 37ºC for
456 2h, after which bacteria were diluted with PBS and plated for CFU determination.

457 **FM1-43 staining.** *S. aureus* WT and mutant strains grown to OD_{600} of 1.0 were
458 centrifuged, and pellets were resuspended in PBS supplemented with 1 µg/mL FM1-
459 43 (Invitrogen). After incubation for 15 min in the dark at 37°C with shaking, cells were
460 washed once with PBS. Fluorescence was quantified using a FLUOstar OMEGA plate
461 reader (BMG Labtech, UK) at excitation and emission wavelengths of 482 nm and 620
462 nm, respectively.

463 **DiIC12 staining.** O/N bacterial cultures were diluted to an OD_{600} of 0.15 in TSB with
464 1 µg/mL 1,1′-didodecyl-3,3,3′,3′-tetramethylindocarbocyanine perchlorate (DiIC12)
465 (Invitrogen). Cultures were grown to an OD_{600} of 1.0, centrifuged and washed twice
466 with fresh TSB. Samples were spotted on to agarose pads and imaged using a Leica
467 DMi8 widefield microscope (Leica Microsystems, UK). Acquired images were
468 analysed with the ImageJ processing package, Fiji.

469 **Growth curves.** O/N bacterial cultures were diluted to an OD_{600} of 0.05 in plain TSB
470 or TSB supplemented with fatty acids. Bacteria were then grown in a 96-well plate with
471 shaking, and the OD_{600} was measured every 15 mins with a FLUOstar OMEGA plate
472 reader (BMG Labtech, UK).

Synthesis of azide functionalized linoleic acid. A 2-step synthesis was used to obtain N^6-diazo-N^2-((9Z,12Z)-octadeca-9,12-dienoyl)lysine, N_3-LA (azide-LA). LA was first functionalized with *N*-hydroxysuccinimide (NHS) in anhydrous dimethyl formamide (DMF) in presence of *N*-(3-dimethylaminopropyl)-*N*'-ethylcarbodiimide hydrochloride. The solvent was then removed and replaced by dicholoromethane (DCM), following which the reaction mixture was washed with water and dried over magnesium sulphate. The product, 2,5-dioxopyrrolidin-1-yl (9Z,12Z)-octadeca-9,12-dienoate (NHS-LA), was analysed using ^{1}H nuclear magnetic resonance (NMR) spectroscopy (Fig. S10A) and mass spectrometry (MS). MS: $[M+Na]^+$ 400.5 (calculated), 400.5 (found).

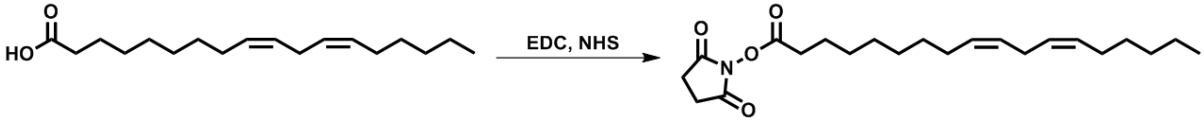

NHS-LA was left O/N at room temperature (RT) to react with L-azidolysine hydrochloride in anhydrous DMF, and produce azide-LA.

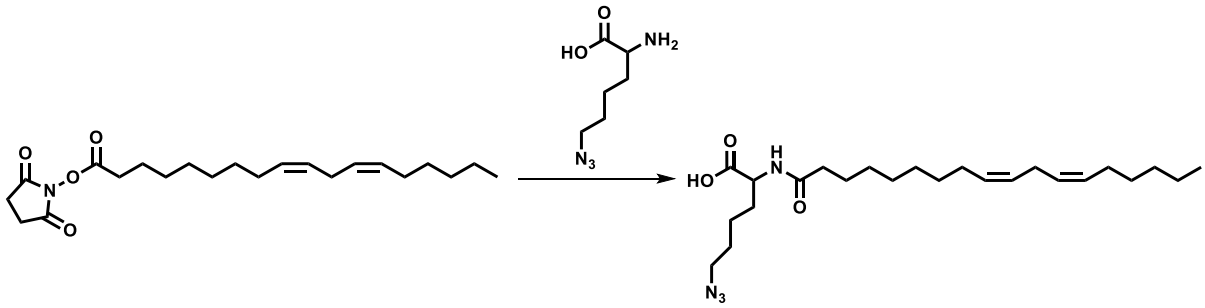

DMF was then removed, the reaction mixture precipitated in water, and dried under vacuum to obtain a clear oil. The composition of the oil was confirmed as being a mixture of azide-LA and unmodified LA (20% and 80%, respectively) based on ^{1}H NMR (Fig. S10B) and MS data. MS: $[LA-H]^-$ 279.5 (calculated), 279.2 (found), $[M-H]^-$ 433.3 (calculated), 433.6 (found).

Binding assays with azide-LA and click chemistry. *S. aureus* USA300 JE2 WT, Δ*essC*, and Δ*esxC*, grown to OD1, were treated with 10 µM azide-LA for 15 min at 37ºC with shaking. The samples were then centrifuged, and the bacterial pellets resuspended in PBS supplemented with 4 µg/mL Click-iT™ Alexa Fluor™ 488 sDIBO alkyne (Life Technologies LTD, UK). After incubation at 25ºC for 1h with shaking, bacteria were washed with PBS, and binding to azide-LA was quantified by measuring fluorescence using a FLUOstar OMEGA plate reader (BMG Labtech, UK). The samples imaged with a microscope were additionally stained with 3 µM propidium iodide, following click chemistry. Bacteria stained with Click-iT™ Alexa Fluor™ 488 sDIBO alkyne and 3 µM propidium iodide were immobilized on agarose-covered glass slides, and viewed with a Leica DMi8 widefield microscope (Leica Microsystems LTD, UK). Images were analysed with the ImageJ processing package Fiji (Schindelin *et al.*, 2012).

Live/Dead Staining. Bacteria grown to $OD6_{00}$ of 1.0, were treated with 80 µM linoleic acid for 15 min at 37°C with shaking. The samples were then centrifuged, and the bacterial pellets resuspended in PBS and supplemented with a 1:1 ratio of 2X LIVE/DEAD solution (6 µM SYTO-9 stain and 30 µM propidium iodide) from LIVE/DEAD® BacLight kit (Invitrogen). After incubation in the dark for 15 min, bacteria were washed with PBS, spotted on to agarose pads and imaged using a Leica DMi8 widefield microscope (Leica Microsystems, UK). Acquired images were analysed with the ImageJ processing package, Fiji.

Lipid extraction and analyses. Lipids were extracted from bacterial cultures as described elsewhere (Smith *et al.*, 2019). Briefly, bacteria were grown to OD1 in TSB or TSB supplemented with 10 µM LA, centrifuged in a 2 mL glass Chromacol vial (Thermo Scientific), and resuspended in 0.5 mL MS grade methanol (Sigma-Aldrich).

MS grade chloroform was then used to extract lipids. The extracted lipids were dried under nitrogen gas with a Techne sample concentrator (Staffordshire, UK), and the lipid pellets resuspended in 1 mL acetonitrile. The samples were then analysed by LC-MS with a Dionex 3400RS HPLC coupled to an amaZon SL quadrupole ion trap mass spectrometer (Bruker Scientific) via an electrospray ionisation interface. Both positive and negative ionisation modes were used for sample analyses. The Bruker Compass software package was utilized for data analyses, using DataAnalysis for peak identification and characterization of lipid class, and QuantAnalysis for quantification of the relative abundance of distinct PG species to total PG species.

Cell shaving for surface proteome analysis. *S. aureus* USA300 JE2 WT grown to OD1 and Δ*esxC* were washed three times before being treated with Proteomics grade trypsin from porcine pancreas (Sigma-Aldrich, UK) for 15 min as described (Solis *et al.*, 2014). The samples were then centrifuged at 1000 × *g* for 15 min, and the bacterial pellets discarded while supernatants were filtered through a 0.2 µM filter. The freshly prepared peptides were frozen (-20ºC) until 2 additional, independent biological replicates per strain were prepared.

Cellular proteomics. *S. aureus* strains were grown O/N at 37ºC on tryptic soy agar plates. The next day, single colonies were used to inoculate 10 mL plain TSB or TSB with 10 µM LA. Cultures were grown at 37ºC with 180-rpm shaking until an OD_{600} of 3.2 ± 0.2 was reached. The bacteria were then centrifuged, washed with PBS, and resuspended in lysis buffer (PBS, 250 mM sucrose, 1 mM EDTA, and 50 µg/mL lysostaphin) supplemented with cOmplete™, mini, EDTA-free protease inhibitor cocktail (Sigma-Aldrich, UK). After 15 min incubation at 37ºC, cells were lysed mechanically with silica spheres (Lysing Matrix B, Fischer Scientific, UK) in a fast-prep shaker as described previously (Mielich-Suss *et al.*, 2017). Samples were then

542 centrifuged, and the supernatants transferred to fresh tubes, where proteins were
543 reduced and alkylated for 20 min at 70ºC with 10 mM TCEP (tris(2-
544 carboxyethyl)phosphine) and 40 mM CAA (2-chloroacetamide), respectively. Next, the
545 solvent was exchanged first to 8M urea buffer then to 50 mM ammonium bicarbonate
546 (ABC). Proteins were digested O/N at 37ºC with mass spectrometry grade lysyl
547 endopeptidase LysC and sequencing grade modified trypsin (Promega LTD, UK).

548 **Preparation of culture supernatant for proteomics analysis.** *S. aureus* strains
549 were grown to an OD_{600} of 3 in TSB. After centrifugation of cultures, supernatants were
550 sterile-filtered and incubated at 4°C overnight with 10% trichloroacetic acid and 50 µM
551 sodium deoxycholate in presence of one cOmplete™, Mini, EDTA-free Protease
552 Inhibitor Cocktail tablet (Sigma-Aldrich, UK). The precipitated proteins (10 000 × *g* at
553 4ºC for 15 min) were gently washed with acetone and dry at RT for 10 min. After
554 denaturation, proteins were run on a gel until all the proteins had moved from the
555 stacking gel to the resolving gel. The gel was then stained with Instant*Blue*™ (Sigma-
556 Aldrich, UK) for 3 h, after which the protein bands were excised and diced. Proteins
557 were in-gel digested with trypsin as recently described(Goodman *et al.*, 2018). Briefly,
558 proteins were reduced and alkylated for 5 min at 70ºC with 10 mM TCEP and 40 mM
559 CAA, respectively. Tryptic digestion was carried out at O/N at 37°C in 50 mM ABC.

560 **Label-free protein quantification.** Peptides prepared for proteome analyses were
561 desalted and concentrated with a C18 cartridge in 40 µL MS buffer (2% acetonitrile
562 plus 0.1% trifluoroacetic acid). For each sample, 20 µL were analysed by nanoLC-
563 ESI-MS/MS using the Ultimate 3000/Orbitrap Fusion instrumentation (Thermo
564 Scientific), and a 90-minute LC separation on a 50 cm column. The data were used to
565 interrogate the Uniprot *Staphylococcus aureus* USA300 database UP000001939, and
566 the common contaminant database from MaxQuant (Cox *et al.*, 2014). MaxQuant

software was used for protein identification and quantification using default settings. Intensities were log_2-tansformed with the Perseus software, and proteins with one or no valid value for every sample in triplicate were filtered. For surfome data, the removeBatchEffect function of the limma R package (Ritchie *et al.*, 2015) was used to remove differences accounting for variation in shaving efficiency done on three different days for all the biological replicates. Missing values in cellular proteomics data were imputed on R. Specifically, for each sample, the imputed value was either the lowest intensity across all samples if at least two biological replicates had missing values or the average of two valid values if only one was missing.

ROS measurement. Chemical hydrolysis of 2,7-dichlorofluorescein diacetate (Sigma-Aldrich) was performed to acquire a final dichlorofluorescein (DCF) reagent yield of 50 µM. Briefly, 0.5 ml of 5 mM DCF-DA (dissolved in 100% ethanol), was reacted with 2 ml of 0.1 N NaOH at RT for 30 min. The reaction was stopped using 7.5 mL 10X PBS pH 7.4 (without calcium and magnesium; Gibco). Bacteria grown to OD_{600} of 1.0 were treated with 10µM linoleic acid or left untreated for 15 min at 37°C shaking and 1 mL of this culture was centrifuged. Cells were resuspended in 100 µL of DCF reagent and incubated for 40 min in the dark at RT. Fluorescence was measured using a FLUOstar OMEGA plate reader (BMG Labtech, UK) at an excitation wavelength of 482 nm and emission wavelength of 520 nm.

Data availability statement. The mass spectrometry proteomics data have been deposited to the ProteomeXchange Consortium via the PRIDE (Perez-Riverol *et al.*, 2019) partner repository with the dataset identifier PXD013081 and 10.6019/PXD013081. Cellular proteomic and surface proteome samples are labelled MS18-193 and MS17-185, respectively.

Statistical analyses. Except for the proteomics results, the statistical tests were performed with GraphPad Prism 8.0 as indicated in the Figure legends, with *P* values < 0.05 considered significant. A paired two-tailed Student's t-test or a paired Mann-Whitney U test was used for pairwise comparisons. An ordinary one-way analysis of variance (ANOVA) with Dunnett's multiple comparisons test or a Kruskal-Wallis test with Dunn's multiple comparisons test was applied to data form three or more groups. The fold changes and *P* values of the proteomics data were calculated with the R package limma (Ritchie *et al.*, 2015), with USA300 JE2 WT or bacteria grown without LA as references. These fold changes and *P* values were used by the R package piano (Varemo *et al.*, 2013) to compute the enrichment of gene ontology (GO) terms.

Acknowledgments

We thank Professor Tracy Palmer (Newcastle University) and Professor Olaf Scheewind (University of Chicago) for providing us *S. aureus* strains and reagents. We thank GSK, Siena, Italy for providing the *esxA*, *esxB* mutant strains used in this study. We acknowledge the contribution of the Proteomics Research Technology Platform, University of Warwick. The authors have no conflict of interest to declare.

References

Alnaseri, H., Arsic, B., Schneider, J.E., Kaiser, J.C., Scinocca, Z.C., Heinrichs, D.E., and McGavin, M.J. (2015) Inducible Expression of a Resistance-Nodulation-Division-Type Efflux Pump in Staphylococcus aureus Provides Resistance to Linoleic and Arachidonic Acids. *J Bacteriol* **197**: 1893-1905.

Aly, K.A., Anderson, M., Ohr, R.J., and Missiakas, D. (2017) Isolation of a Membrane Protein Complex for Type VII Secretion in Staphylococcus aureus. *J Bacteriol* **199**.

Anderson, M., Aly, K.A., Chen, Y.H., and Missiakas, D. (2013) Secretion of atypical protein substrates by the ESAT-6 secretion system of Staphylococcus aureus. *Mol Microbiol* **90**: 734-743.

Anderson, M., Chen, Y.H., Butler, E.K., and Missiakas, D.M. (2011) EsaD, a secretion factor for the Ess pathway in Staphylococcus aureus. *J Bacteriol* **193**: 1583-1589.

Anderson, M., Ohr, R.J., Aly, K.A., Nocadello, S., Kim, H.K., Schneewind, C.E., Schneewind, O., and Missiakas, D. (2017) EssE Promotes Staphylococcus aureus ESS-Dependent Protein Secretion To Modify Host Immune Responses during Infection. *J Bacteriol* **199**.

Arsic, B., Zhu, Y., Heinrichs, D.E., and McGavin, M.J. (2012) Induction of the staphylococcal proteolytic cascade by antimicrobial fatty acids in community acquired methicillin resistant Staphylococcus aureus. *PLoS One* **7**: e45952.

Bach, J.N., and Bramkamp, M. (2013) Flotillins functionally organize the bacterial membrane. *Mol Microbiol* **88**: 1205-1217.

Bae, T., and Schneewind, O. (2006) Allelic replacement in Staphylococcus aureus with inducible counter-selection. *Plasmid* **55**: 58-63.

Binns, D., Dimmer, E., Huntley, R., Barrell, D., O'Donovan, C., and Apweiler, R. (2009) QuickGO: a web-based tool for Gene Ontology searching. *Bioinformatics* **25**: 3045-3046.

639 Bobrovskyy, M., Willing, S.E., Schneewind, O., and Missiakas, D. (2018) EssH peptidoglycan
640 hydrolase enables Staphylococcus aureus type VII secretion across the bacterial cell
641 wall envelope. *J Bacteriol*.
642 Burts, M.L., DeDent, A.C., and Missiakas, D.M. (2008) EsaC substrate for the ESAT-6
643 secretion pathway and its role in persistent infections of Staphylococcus aureus. *Mol*
644 *Microbiol* **69**: 736-746.
645 Burts, M.L., Williams, W.A., DeBord, K., and Missiakas, D.M. (2005) EsxA and EsxB are
646 secreted by an ESAT-6-like system that is required for the pathogenesis of
647 Staphylococcus aureus infections. *Proc Natl Acad Sci U S A* **102**: 1169-1174.
648 Cao, Z., Casabona, M.G., Kneuper, H., Chalmers, J.D., and Palmer, T. (2016) The type VII
649 secretion system of Staphylococcus aureus secretes a nuclease toxin that targets
650 competitor bacteria. *Nat Microbiol* **2**: 16183.
651 Cartron, M.L., England, S.R., Chiriac, A.I., Josten, M., Turner, R., Rauter, Y., Hurd, A., Sahl,
652 H.G., Jones, S., and Foster, S.J. (2014) Bactericidal activity of the human skin fatty
653 acid cis-6-hexadecanoic acid on Staphylococcus aureus. *Antimicrob Agents*
654 *Chemother* **58**: 3599-3609.
655 Casabona, M.G., Buchanan, G., Zoltner, M., Harkins, C.P., Holden, M.T.G., and Palmer, T.
656 (2017a) Functional analysis of the EsaB component of the Staphylococcus aureus
657 Type VII secretion system. *Microbiology*.
658 Casabona, M.G., Kneuper, H., Alferes de Lima, D., Harkins, C.P., Zoltner, M., Hjerde, E.,
659 Holden, M.T.G., and Palmer, T. (2017b) Haem-iron plays a key role in the regulation
660 of the Ess/type VII secretion system of Staphylococcus aureus RN6390. *Microbiology*
661 **163**: 1839-1850.
662 Cassat, J., Dunman, P.M., Murphy, E., Projan, S.J., Beenken, K.E., Palm, K.J., Yang, S.J.,
663 Rice, K.C., Bayles, K.W., and Smeltzer, M.S. (2006) Transcriptional profiling of a
664 Staphylococcus aureus clinical isolate and its isogenic agr and sarA mutants reveals
665 global differences in comparison to the laboratory strain RN6390. *Microbiology* **152**:
666 3075-3090.

667 Chamberlain, N.R., Mehrtens, B.G., Xiong, Z., Kapral, F.A., Boardman, J.L., and Rearick, J.I.
668 (1991) Correlation of carotenoid production, decreased membrane fluidity, and
669 resistance to oleic acid killing in Staphylococcus aureus 18Z. *Infect Immun* **59**: 4332-
670 4337.
671 Clarke, S.R., Mohamed, R., Bian, L., Routh, A.F., Kokai-Kun, J.F., Mond, J.J., Tarkowski, A.,
672 and Foster, S.J. (2007) The Staphylococcus aureus surface protein IsdA mediates
673 resistance to innate defenses of human skin. *Cell Host Microbe* **1**: 199-212.
674 Conrad, W.H., Osman, M.M., Shanahan, J.K., Chu, F., Takaki, K.K., Cameron, J., Hopkinson-
675 Woolley, D., Brosch, R., and Ramakrishnan, L. (2017) Mycobacterial ESX-1 secretion
676 system mediates host cell lysis through bacterium contact-dependent gross membrane
677 disruptions. *Proc Natl Acad Sci U S A* **114**: 1371-1376.
678 Cox, J., Hein, M.Y., Luber, C.A., Paron, I., Nagaraj, N., and Mann, M. (2014) Accurate
679 proteome-wide label-free quantification by delayed normalization and maximal peptide
680 ratio extraction, termed MaxLFQ. *Mol Cell Proteomics* **13**: 2513-2526.
681 Cruciani, M., Etna, M.P., Camilli, R., Giacomini, E., Percario, Z.A., Severa, M., Sandini, S.,
682 Rizzo, F., Brandi, V., Balsamo, G., Polticelli, F., Affabris, E., Pantosti, A., Bagnoli, F.,
683 and Coccia, E.M. (2017) Staphylococcus aureus Esx Factors Control Human Dendritic
684 Cell Functions Conditioning Th1/Th17 Response. *Front Cell Infect Microbiol* **7**: 330.
685 Delekta, P.C., Shook, J.C., Lydic, T.A., Mulks, M.H., and Hammer, N.D. (2018)
686 Staphylococcus aureus utilizes host-derived lipoprotein particles as sources of
687 exogenous fatty acids. *J Bacteriol*.
688 Dreisbach, A., Hempel, K., Buist, G., Hecker, M., Becher, D., and van Dijl, J.M. (2010) Profiling
689 the surfacome of Staphylococcus aureus. *Proteomics* **10**: 3082-3096.
690 Fey, P.D., Endres, J.L., Yajjala, V.K., Widhelm, T.J., Boissy, R.J., Bose, J.L., and Bayles, K.W.
691 (2013) A genetic resource for rapid and comprehensive phenotype screening of
692 nonessential Staphylococcus aureus genes. *MBio* **4**: e00537-00512.
693 Garcia-Fernandez, E., Koch, G., Wagner, R.M., Fekete, A., Stengel, S.T., Schneider, J.,
694 Mielich-Suss, B., Geibel, S., Markert, S.M., Stigloher, C., and Lopez, D. (2017)

695 Membrane Microdomain Disassembly Inhibits MRSA Antibiotic Resistance. *Cell* **171**:
696 1354-1367 e1320.
697 Geiger, T., Francois, P., Liebeke, M., Fraunholz, M., Goerke, C., Krismer, B., Schrenzel, J.,
698 Lalk, M., and Wolz, C. (2012) The stringent response of Staphylococcus aureus and
699 its impact on survival after phagocytosis through the induction of intracellular PSMs
700 expression. *PLoS Pathog* **8**: e1003016.
701 George, S.E., Hrubesch, J., Breuing, I., Vetter, N., Korn, N., Hennemann, K., Bleul, L.,
702 Willmann, M., Ebner, P., Gotz, F., and Wolz, C. (2019) Oxidative stress drives the
703 selection of quorum sensing mutants in the Staphylococcus aureus population. *Proc*
704 *Natl Acad Sci U S A* **116**: 19145-19154.
705 Giachino, P., Engelmann, S., and Bischoff, M. (2001) Sigma(B) activity depends on RsbU in
706 Staphylococcus aureus. *J Bacteriol* **183**: 1843-1852.
707 Goodman, J.K., Zampronio, C.G., Jones, A.M.E., and Hernandez-Fernaud, J.R. (2018)
708 Updates of the In-Gel Digestion Method for Protein Analysis by Mass Spectrometry.
709 *Proteomics* **18**: e1800236.
710 Gordon, R.J., and Lowy, F.D. (2008) Pathogenesis of methicillin-resistant Staphylococcus
711 aureus infection. *Clin Infect Dis* **46 Suppl 5**: S350-359.
712 Greenway, D.L., and Dyke, K.G. (1979) Mechanism of the inhibitory action of linoleic acid on
713 the growth of Staphylococcus aureus. *J Gen Microbiol* **115**: 233-245.
714 Groicher, K.H., Firek, B.A., Fujimoto, D.F., and Bayles, K.W. (2000) The Staphylococcus
715 aureus lrgAB operon modulates murein hydrolase activity and penicillin tolerance. *J*
716 *Bacteriol* **182**: 1794-1801.
717 Hempel, K., Herbst, F.A., Moche, M., Hecker, M., and Becher, D. (2011) Quantitative
718 proteomic view on secreted, cell surface-associated, and cytoplasmic proteins of the
719 methicillin-resistant human pathogen Staphylococcus aureus under iron-limited
720 conditions. *J Proteome Res* **10**: 1657-1666.
721 Horsburgh, M.J., Ingham, E., and Foster, S.J. (2001) In Staphylococcus aureus, fur is an
722 interactive regulator with PerR, contributes to virulence, and Is necessary for oxidative

723 stress resistance through positive regulation of catalase and iron homeostasis. *J*
724 *Bacteriol* **183**: 468-475.
725 Ishii, K., Adachi, T., Yasukawa, J., Suzuki, Y., Hamamoto, H., and Sekimizu, K. (2014)
726 Induction of virulence gene expression in Staphylococcus aureus by pulmonary
727 surfactant. *Infect Immun* **82**: 1500-1510.
728 Jager, F., Kneuper, H., and Palmer, T. (2018) EssC is a specificity determinant for
729 Staphylococcus aureus type VII secretion. *Microbiology* **164**: 816-820.
730 Johnson, M., Sengupta, M., Purves, J., Tarrant, E., Williams, P.H., Cockayne, A., Muthaiyan,
731 A., Stephenson, R., Ledala, N., Wilkinson, B.J., Jayaswal, R.K., and Morrissey, J.A.
732 (2011) Fur is required for the activation of virulence gene expression through the
733 induction of the sae regulatory system in Staphylococcus aureus. *Int J Med Microbiol*
734 **301**: 44-52.
735 Kelsey, J.A., Bayles, K.W., Shafii, B., and McGuire, M.A. (2006) Fatty acids and
736 monoacylglycerols inhibit growth of Staphylococcus aureus. *Lipids* **41**: 951-961.
737 Kenny, J.G., Ward, D., Josefsson, E., Jonsson, I.M., Hinds, J., Rees, H.H., Lindsay, J.A.,
738 Tarkowski, A., and Horsburgh, M.J. (2009) The Staphylococcus aureus response to
739 unsaturated long chain free fatty acids: survival mechanisms and virulence
740 implications. *PLoS One* **4**: e4344.
741 Kneuper, H., Cao, Z.P., Twomey, K.B., Zoltner, M., Jager, F., Cargill, J.S., Chalmers, J., van
742 der Kooi-Pol, M.M., van Dijl, J.M., Ryan, R.P., Hunter, W.N., and Palmer, T. (2014)
743 Heterogeneity in ess transcriptional organization and variable contribution of the
744 Ess/Type VII protein secretion system to virulence across closely related
745 Staphylocccus aureus strains. *Mol Microbiol* **93**: 928-943.
746 Kohler, T., Weidenmaier, C., and Peschel, A. (2009) Wall teichoic acid protects
747 Staphylococcus aureus against antimicrobial fatty acids from human skin. *J Bacteriol*
748 **191**: 4482-4484.
749 Korea, C.G., Balsamo, G., Pezzicoli, A., Merakou, C., Tavarini, S., Bagnoli, F., Serruto, D.,
750 and Unnikrishnan, M. (2014) Staphylococcal Esx proteins modulate apoptosis and

release of intracellular Staphylococcus aureus during infection in epithelial cells. *Infect Immun* **82**: 4144-4153.

Lee, A.S., de Lencastre, H., Garau, J., Kluytmans, J., Malhotra-Kumar, S., Peschel, A., and Harbarth, S. (2018) Methicillin-resistant Staphylococcus aureus. *Nat Rev Dis Primers* **4**: 18033.

Liang, X., Zheng, L., Landwehr, C., Lunsford, D., Holmes, D., and Ji, Y. (2005) Global regulation of gene expression by ArlRS, a two-component signal transduction regulatory system of Staphylococcus aureus. *J Bacteriol* **187**: 5486-5492.

Lopez, M.S., Tan, I.S., Yan, D., Kang, J., McCreary, M., Modrusan, Z., Austin, C.D., Xu, M., and Brown, E.J. (2017) Host-derived fatty acids activate type VII secretion in Staphylococcus aureus. *Proc Natl Acad Sci U S A* **114**: 11223-11228.

Mashruwala, A.A., Guchte, A.V., and Boyd, J.M. (2017) Impaired respiration elicits SrrAB-dependent programmed cell lysis and biofilm formation in Staphylococcus aureus. *Elife* **6**.

Mielich-Suss, B., Wagner, R.M., Mietrach, N., Hertlein, T., Marincola, G., Ohlsen, K., Geibel, S., and Lopez, D. (2017) Flotillin scaffold activity contributes to type VII secretion system assembly in Staphylococcus aureus. *PLoS Pathog* **13**: e1006728.

Moran, J.C., Alorabi, J.A., and Horsburgh, M.J. (2017) Comparative Transcriptomics Reveals Discrete Survival Responses of S. aureus and S. epidermidis to Sapienic Acid. *Front Microbiol* **8**: 33.

Neumann, Y., Ohlsen, K., Donat, S., Engelmann, S., Kusch, H., Albrecht, D., Cartron, M., Hurd, A., and Foster, S.J. (2015) The effect of skin fatty acids on Staphylococcus aureus. *Arch Microbiol* **197**: 245-267.

Nguyen, M.T., Hanzelmann, D., Hartner, T., Peschel, A., and Gotz, F. (2016) Skin-Specific Unsaturated Fatty Acids Boost the Staphylococcus aureus Innate Immune Response. *Infect Immun* **84**: 205-215.

Ohr, R.J., Anderson, M., Shi, M., Schneewind, O., and Missiakas, D. (2017) EssD, a Nuclease Effector of the Staphylococcus aureus ESS Pathway. *J Bacteriol* **199**.

779 Parsons, J.B., Broussard, T.C., Bose, J.L., Rosch, J.W., Jackson, P., Subramanian, C., and
780 Rock, C.O. (2014) Identification of a two-component fatty acid kinase responsible for
781 host fatty acid incorporation by Staphylococcus aureus. *Proc Natl Acad Sci U S A* **111**:
782 10532-10537.
783 Parsons, J.B., Frank, M.W., Subramanian, C., Saenkham, P., and Rock, C.O. (2011)
784 Metabolic basis for the differential susceptibility of Gram-positive pathogens to fatty
785 acid synthesis inhibitors. *Proc Natl Acad Sci U S A* **108**: 15378-15383.
786 Parsons, J.B., Yao, J., Frank, M.W., Jackson, P., and Rock, C.O. (2012) Membrane disruption
787 by antimicrobial fatty acids releases low-molecular-weight proteins from
788 Staphylococcus aureus. *J Bacteriol* **194**: 5294-5304.
789 Pasztor, L., Ziebandt, A.K., Nega, M., Schlag, M., Haase, S., Franz-Wachtel, M., Madlung, J.,
790 Nordheim, A., Heinrichs, D.E., and Gotz, F. (2010) Staphylococcal major autolysin (Atl)
791 is involved in excretion of cytoplasmic proteins. *J Biol Chem* **285**: 36794-36803.
792 Patton, T.G., Yang, S.J., and Bayles, K.W. (2006) The role of proton motive force in expression
793 of the Staphylococcus aureus cid and lrg operons. *Mol Microbiol* **59**: 1395-1404.
794 Perez-Riverol, Y., Csordas, A., Bai, J., Bernal-Llinares, M., Hewapathirana, S., Kundu, D.J.,
795 Inuganti, A., Griss, J., Mayer, G., Eisenacher, M., Perez, E., Uszkoreit, J., Pfeuffer, J.,
796 Sachsenberg, T., Yilmaz, S., Tiwary, S., Cox, J., Audain, E., Walzer, M., Jarnuczak,
797 A.F., Ternent, T., Brazma, A., and Vizcaino, J.A. (2019) The PRIDE database and
798 related tools and resources in 2019: improving support for quantification data. *Nucleic*
799 *Acids Res* **47**: D442-D450.
800 Pulschen, A.A., Sastre, D.E., Machinandiarena, F., Crotta Asis, A., Albanesi, D., de Mendoza,
801 D., and Gueiros-Filho, F.J. (2017) The stringent response plays a key role in Bacillus
802 subtilis survival of fatty acid starvation. *Mol Microbiol* **103**: 698-712.
803 Ritchie, M.E., Phipson, B., Wu, D., Hu, Y., Law, C.W., Shi, W., and Smyth, G.K. (2015) limma
804 powers differential expression analyses for RNA-sequencing and microarray studies.
805 *Nucleic Acids Res* **43**: e47.

806 Saeloh, D., Tipmanee, V., Jim, K.K., Dekker, M.P., Bitter, W., Voravuthikunchai, S.P., Wenzel,
807 M., and Hamoen, L.W. (2018) The novel antibiotic rhodomyrtone traps membrane
808 proteins in vesicles with increased fluidity. *PLoS Pathog* **14**: e1006876.
809 Schindelin, J., Arganda-Carreras, I., Frise, E., Kaynig, V., Longair, M., Pietzsch, T., Preibisch,
810 S., Rueden, C., Saalfeld, S., Schmid, B., Tinevez, J.Y., White, D.J., Hartenstein, V.,
811 Eliceiri, K., Tomancak, P., and Cardona, A. (2012) Fiji: an open-source platform for
812 biological-image analysis. *Nat Methods* **9**: 676-682.
813 Sen, S., Sirobhushanam, S., Johnson, S.R., Song, Y., Tefft, R., Gatto, C., and Wilkinson, B.J.
814 (2016) Growth-Environment Dependent Modulation of Staphylococcus aureus
815 Branched-Chain to Straight-Chain Fatty Acid Ratio and Incorporation of Unsaturated
816 Fatty Acids. *PLoS One* **11**: e0165300.
817 Smith, A.F., Rihtman, B., Stirrup, R., Silvano, E., Mausz, M.A., Scanlan, D.J., and Chen, Y.
818 (2019) Elucidation of glutamine lipid biosynthesis in marine bacteria reveals its
819 importance under phosphorus deplete growth in Rhodobacteraceae. *ISME J* **13**: 39-
820 49.
821 Solis, N., Parker, B.L., Kwong, S.M., Robinson, G., Firth, N., and Cordwell, S.J. (2014)
822 Staphylococcus aureus surface proteins involved in adaptation to oxacillin identified
823 using a novel cell shaving approach. *J Proteome Res* **13**: 2954-2972.
824 Tiwari, K.B., Gatto, C., and Wilkinson, B.J. (2018) Interrelationships between Fatty Acid
825 Composition, Staphyloxanthin Content, Fluidity, and Carbon Flow in the
826 Staphylococcus aureus Membrane. *Molecules* **23**.
827 Tong, S.Y., Davis, J.S., Eichenberger, E., Holland, T.L., and Fowler, V.G., Jr. (2015)
828 Staphylococcus aureus infections: epidemiology, pathophysiology, clinical
829 manifestations, and management. *Clin Microbiol Rev* **28**: 603-661.
830 Truong-Bolduc, Q.C., Villet, R.A., Estabrooks, Z.A., and Hooper, D.C. (2014) Native efflux
831 pumps contribute resistance to antimicrobials of skin and the ability of Staphylococcus
832 aureus to colonize skin. *J Infect Dis* **209**: 1485-1493.

833 Unnikrishnan, M., Constantinidou, C., Palmer, T., and Pallen, M.J. (2017) The Enigmatic Esx
834 Proteins: Looking Beyond Mycobacteria. *Trends Microbiol* **25**: 192-204.
835 Varemo, L., Nielsen, J., and Nookaew, I. (2013) Enriching the gene set analysis of genome-
836 wide data by incorporating directionality of gene expression and combining statistical
837 hypotheses and methods. *Nucleic Acids Res* **41**: 4378-4391.
838 Ventura, C.L., Malachowa, N., Hammer, C.H., Nardone, G.A., Robinson, M.A., Kobayashi,
839 S.D., and DeLeo, F.R. (2010) Identification of a novel Staphylococcus aureus two-
840 component leukotoxin using cell surface proteomics. *PLoS One* **5**: e11634.
841 von Eiff, C., Becker, K., Machka, K., Stammer, H., and Peters, G. (2001) Nasal carriage as a
842 source of Staphylococcus aureus bacteremia. Study Group. *N Engl J Med* **344**: 11-16.
843 Wang, Y., Hu, M., Liu, Q., Qin, J., Dai, Y., He, L., Li, T., Zheng, B., Zhou, F., Yu, K., Fang, J.,
844 Liu, X., Otto, M., and Li, M. (2016) Role of the ESAT-6 secretion system in virulence
845 of the emerging community-associated Staphylococcus aureus lineage ST398. *Sci*
846 *Rep* **6**: 25163.
847 Warne, B., Harkins, C.P., Harris, S.R., Vatsiou, A., Stanley-Wall, N., Parkhill, J., Peacock,
848 S.J., Palmer, T., and Holden, M.T. (2016) The Ess/Type VII secretion system of
849 Staphylococcus aureus shows unexpected genetic diversity. *BMC Genomics* **17**: 222.
850 Wood, T.E., Howard, S.A., Forster, A., Nolan, L.M., Manoli, E., Bullen, N.P., Yau, H.C.L.,
851 Hachani, A., Hayward, R.D., Whitney, J.C., Vollmer, W., Freemont, P.S., and Filloux,
852 A. (2019) The Pseudomonas aeruginosa T6SS Delivers a Periplasmic Toxin that
853 Disrupts Bacterial Cell Morphology. *Cell Rep* **29**: 187-201 e187.
854 Zoltner, M., Ng, W.M., Money, J.J., Fyfe, P.K., Kneuper, H., Palmer, T., and Hunter, W.N.
855 (2016) EssC: domain structures inform on the elusive translocation channel in the Type
856 VII secretion system. *Biochem J* **473**: 1941-1952.

857

858 **Figure legends**

859 **Fig. 1. Membrane defects in the absence of EsxC.**

860 **A**. FM1-43 fluorescence of *S. aureus* WT, Δ*essC*, and Δ*esxC* as measured with a
861 plate reader. Means ± standard deviation (SD) are shown, $n = 6$; * indicates $P < 0.05$
862 using a Kruskal-Wallis test with Dunn's test.
863 **B**. Survival of Δ*esxC* or Δ*essC* after a 2h-treatment with 0.1% Triton X-100 relative to
864 the WT. Means are shown; error bars represent standard deviation (SD). $n = 4$, *
865 indicates $P < 0.05$ using a Kruskal-Wallis test with Dunn's test. The panel on the right
866 shows a representative picture of bacteria before and after Triton X-100-treatment.
867 **C**. The membrane fluidity of WT and Δ*esxC* as measured with a pyrene decanoic acid
868 staining-based assay. Mean values are shown; error bars represent standard error of
869 the mean (SEM). $n = 6$, * indicates $P < 0.05$ using a two-tailed t-test.
870 **D**. Widefield micrographs of *S. aureus* WT and Δ*esxC* after growth in TSB to OD_{600} of
871 1.0 in the presence of the lipophilic dye DiIC12. Images are representative of 4
872 independent experiments.

873 **E**. The DiIC12 fluorescence of 80 bacterial clusters from different fields per strain was
874 quantitated with ImageJ. Means ± standard deviation (SD) are shown, $n = 4$; indicates
875 **** $P < 0.0001$, using a Kruskal-Wallis rank test

876 **Fig. 2. Enhanced *S. aureus* growth inhibition by linoleic acid in T7SS mutants.**
877 **A**. *S. aureus* WT USA300, Δ*essC*, and Δ*esxC* were grown in TSB or TSB
878 supplemented with 80 µM of either linoleic (LA) or stearic acid (SA). Means ± standard
879 error of the mean (SEM) are shown.

B. After 14h growth as described in (A) bacteria were serially diluted, and CFU were determined. Mean values are presented, and the error bars represent SD. *n* = 3, ** indicates $P < 0.01$ using one-way ANOVA with Dunnett's test.

C. USA300 WT with the empty pOS1 plasmid (WT pOS1) and USA300 JE2 *esxC* mutant with either pOS1 (Δ*esxC* pOS1) or pOS1-*esxC* (Δ*esxC* pOS1-*esxC*) were grown in TSB or TSB + 80 μM LA as described in (A) followed by CFU estimation. Mean values are shown; error bars represent SD. *n* = 5, ** indicates $P < 0.01$ using one-way ANOVA with Dunnett's test.

D. Newman WT with the empty pOS1 plasmid (WT pOS1) and Newman *esxA* mutant with either pOS1 (Δ*esxA* pOS1) or pOS1-*esxA* (Δ*esxA* p*esxA*) were grown in TSB or TSB + 40 μM LA or SA. Means ± standard error of the mean (SEM) are shown, *n* = 4**.**

Fig. 3. T7SS mutants display increased membrane permeability upon LA binding.

A. Chemical structure of azide functionalised linoleic acid (azide-LA; N^6-diazo-N^2-((9Z,12Z)-octadeca-9,12-dienoyl)lysine, N_3-LA). Highlighted in green is the azido lysine.

B. *S. aureus* USA300 WT, Δ*essC*, and Δ*esxC* were grown with shaking in TSB to OD_{600} of 1.0. Bacteria were then stained for 15 min with 10 μM azide-LA prior to labelling for 1 h with alkyne Alexa Fluor 488. Mean percentage of fluorescence values relative to WT (100%) are presented; error bars represent SD, *n* = 5.

C. Micrographs of bacteria grown in TSB and treated as described in (B) and additionally stained with propidium iodide (PI).

D. ImageJ was used to quantitate PI fluorescence of bacterial clusters from 12 different fields per strain. Each box-and-whisker plot depicts the minimal and maximal PI

intensities, the median is the vertical bar inside the box, which is delimited by the lower and upper quartiles. ** indicates $P < 0.01$ using one-way ANOVA with Dunnett's test.

Fig. 4. T7SS mutants display increased PI staining when treated with LA. Live/Dead staining of *S. aureus* USA300 WT, Δ*essC* or Δ*esxC* mutants after growth to OD_{600} of 1.0, without (**A**) or with treatment with 80μM (**B**) linoleic acid. Images are representative of 3 independent experiments.

C. The ratio of SYTO 9: PI fluorescence (live:dead cells) of 25 different fields per strain was quantitated with ImageJ. Means ± SD are shown, $n = 3$; *** indicates $P < 0.001$, ** indicates $P < 0.01$ using a one-way ANOVA with Tukey's multiple-comparison test

Fig. 5. T7SS mutants are less able to incorporate LA into their phospholipids. Representative HPLC chromatograms of native phosphatidylglycerol (PG) species of *S. aureus* USA300 JE2 WT (**A**) or Δ*esxC* (**B**) grown in TSB (top panel) or in TSB supplemented with 10 μM LA (bottom panel), in negative ionisation mode. Relative quantification of the indicated PG species containing an unsaturated FA in WT, Δ*essC* and Δ*esxC*. C18:2-containing PG species (**C**) and total unsaturated exogenous PG species (**D**) are presented as ratios of total PG species. Mean values are shown; error bars represent SD. $n = 3$, * indicates $P < 0.05$ using one-way ANOVA with Dunnett's test.

Fig. 6. Quantitative proteomics shows altered cellular content and bacterial response to LA in T7SS mutants. *S. aureus* USA300 WT and mutants (Δ*essC* and Δ*esxC*) were grown in TSB or TSB supplemented with LA.

A. Venn diagram showing the number of proteins with altered abundance compared to WT specific to Δ*essC* (23) or Δ*esxC* (10), and common to Δ*essC* and Δ*esxC* (14).

927 **B**. The fourteen proteins that are similarly changed in Δ*essC* and Δ*esxC* mutants are
928 highlighted on a volcano plot.
929 **C**. Volcano plot showing the extensive change in the LA-treated WT compared to WT.
930 **D**. Venn diagram displaying the numbers of proteins with altered relative abundance
931 upon LA challenge of WT (LA.WT), Δ*essC* (LA.dEssC) or Δ*esxC* (LA.dEsxC)
932 compared to the respective untreated samples.

933 **Fig. 7. An altered oxidoreductive response in T7SS mutants in response to LA.**
934 Heatmaps depicting the *P* values of enriched (**A**) or diminished (**B**) molecular functions
935 following a gene set analysis based on GO (gene ontology) annotations. Molecular
936 functions that are changed in at least one strain ($P < 0.05$) following growth in presence
937 of LA are shown. The shades of blue (**A**) or red (**B**) correspond to $-\log_{10}$ (*P* value).
938 ROS levels were measured in cultures of *S. aureus* USA300 JE2 WT, Δ*essC* or Δ*esxC*
939 grown to OD_{600} of 1.0 treated (**C)** with or without LA (**D**) using DCF reagent. Means ±
940 SD are shown N=5. * indicates $P < 0.05$, ** indicates $P < 0.01$, *** indicates $P < 0.001$
941 using the Kruskal-Wallis rank test.

942 **Fig. S1. USA300 JE2 WT and Δ*esxC* strains display similar growth rates.** WT and
943 Δ*esxC* were grown in TSB, and OD_{600} monitored with a Novaspec® Pro
944 spectrophotometer. Data shown are means of three independent experiments, and
945 the error bars indicate the standard errors of the mean.

946 **Fig. S2. EsxC associates with *S. aureus* membrane**. Immunoblot analysis of cell
947 membrane (CM) or cell wall (CW) fractions of WT (USA300), Δ*essC*, and Δ*esxC* with
948 anti-EsxC sera or anti-PBP2a antibodies (loading control).

949 **Fig. S3. Volcano plot of the quantitative proteomic analysis of surface proteins**
950 **in Δ*esxC* compared to WT.** The relative abundance of each protein ($\log_2$ fold change,

951 X-axis) and its statistical significance (*P* value, Y-axis) are shown in the graph.
952 Proteins decreased by more than half in Δ*esxC* (log_2 fold change < -1 and *P* value <
953 0.05) are shown in green.

954 **Fig. S4. *S. aureus* growth inhibition by arachidonic acid is increased in T7SS**
955 **mutants.** *S. aureus* WT USA300, Δ*essC*, and Δ*esxC* were grown in TSB or TSB
956 supplemented with 80 µM arachidonic acid (AA). Means ± standard error of the mean
957 (SEM) are shown, *n* = 3.

958 **Fig. S5. T7SS substrates contribute to resistance to linoleic acid toxicity**.
959 A. *S. aureus* USA300 wild-type (WT) and USA300 *esxA* (Δ*esxA*) or *esxB* (Δ*esxB*)
960 deletion mutants were grown in TSB or TSB supplemented with 80 µM linoleic (LA) or
961 stearic acid (SA).
962 B. *S. aureus* Newman WT and Newman *esxA* (Δ*esxA*) or *esxB* (Δ*esxB*) deletion
963 mutants were grown similarly in TSB or TSB + 40 µM LA or SA.
964 C. Growth curves as described in (A) were done with RN6390 wild-type (WT) and
965 RN6390 *essC* (Δ*essC*) or *esxC* (Δ*esxC*) deletion mutants. Data shown in (A), (B), and
966 (C) are representative of at least three independent experiments.

967 **Fig. S6. USA300 JE2 WT and T7SS mutants display similar lipids.**
968 Representative HPLC chromatograms of the indicated bacteria grown in TSB (A) or in
969 TSB supplemented with LA (B), in negative ionisation mode. Phosphatidylglycerol
970 (PG) is highlighted.
971 C. Representative HPLC chromatograms of native PG species of Δ*essC* grown in TSB
972 (top panel) or in TSB supplemented with LA (bottom panel), in negative ionisation
973 mode.

Fig. S7. LA (C18:2) is elongated and incorporated into *S. aureus* phosphatidylglycerol (PG) species. A-C. Representative mass spectrometry fragmentation spectra for PG species containing unsaturated fatty acids, in negative ionisation mode.

A. PG species with mass 731 m/z, containing C18:2 fatty acid (279 m/z).

B. PG species 759 m/z, containing C20:2 fatty acid (307 m/z)

C. PG species 787 m/z, containing C22:2 fatty acid (335 m/z).

D. and E. Relative quantification of the indicated PG species containing an unsaturated fatty acid in WT, Δ*essC* and Δ*esxC*. C20:2- (D) and C22:2-containing PG species (E) are presented as ratios of total PG species. Data shown are the means and error bars represent SD of three independent experiments.

Fig. S8. USA300 JE2 WT and Δ*esxC* growth similarly in presence of sub-inhibitory amounts of linoleic acid. *S. aureus* WT USA300 and Δ*esxC* were grown in TSB or TSB supplemented with 40 μM linoleic acid (LA). Means ± SEM are shown, $n = 3$.

Fig. S9. Principal component analysis (PCA) of the *S. aureus* cellular proteomic profiles. PCA was performed on all the identified proteins of USA300 JE2 WT and T7SS mutants grown in TSB (untreated) or TSB + LA (LA-treated). Each dot represents a biological replicate.

Fig. S10. ^{1}H NMR spectra of NHS-LA (A) and azide-LA (B) in $CDCl_3$. Both spectra were recorded on a Bruker Advance 300 spectrometer (300 MHz) at 27 °C. The letters indicate the chemical shift δ (in parts per million, ppm) of the protons in each molecule.

Dataset S1. Differentially abundant proteins in WT USA300 JE2 and T7SS mutants in response to linoleic acid.

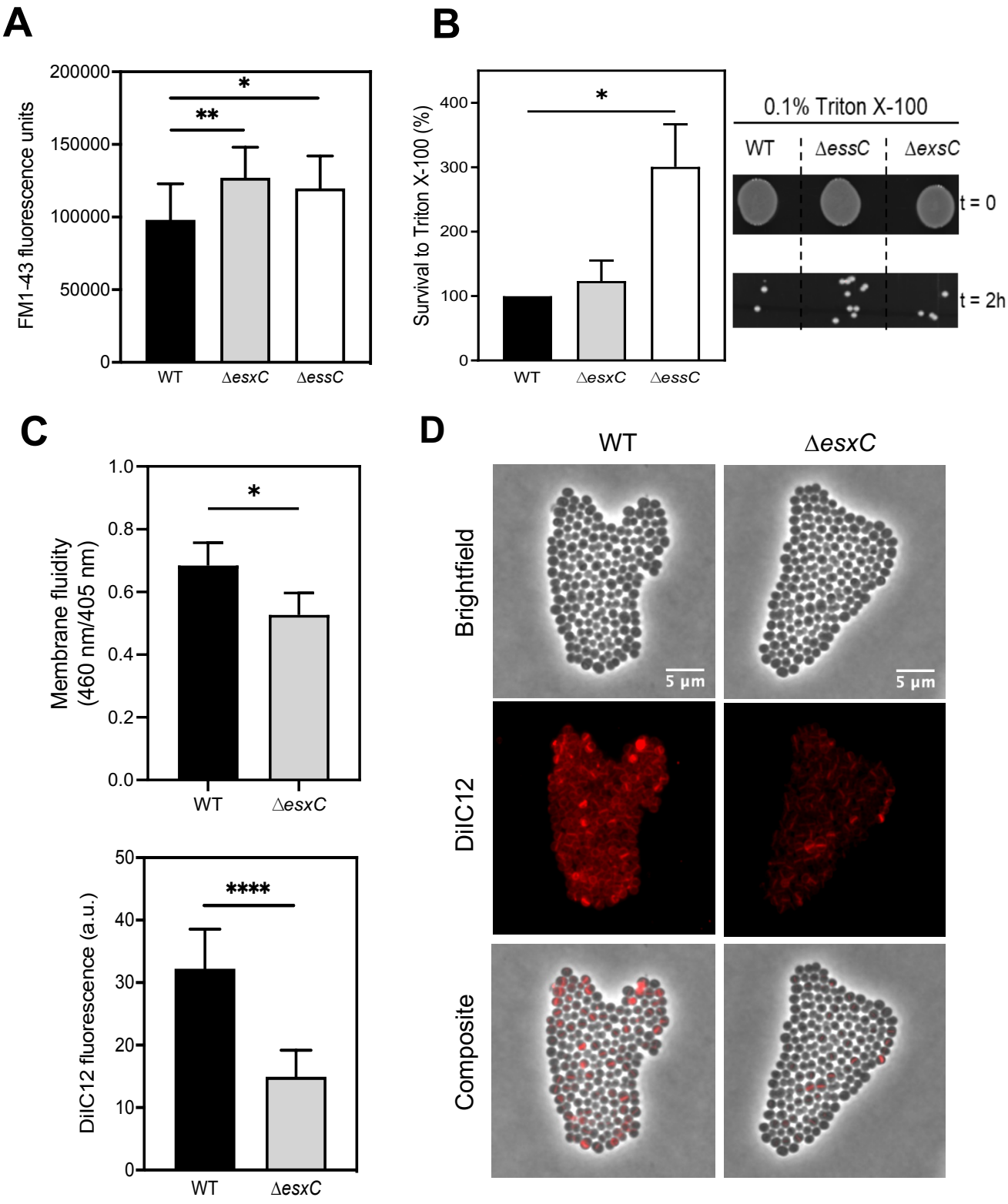
A
FM1-43 fluorescence units
200000
150000
100000
50000
0
*
**
WT
ΔesxC
ΔessC
B
Survival to Triton X-100 (%)
400
300
200
100
0
*
WT
ΔesxC
ΔessC
0.1% Triton X-100
WT
ΔessC
ΔexsC
t = 0
t = 2h
C
Membrane fluidity (460 nm/405 nm)
1.0
0.8
0.6
0.4
0.2
0.0
*
WT
ΔesxC
DiIC12 fluorescence (a.u.)
50
40
30
20
10
0
****
WT
ΔesxC
D
WT
ΔesxC
Brightfield
DiIC12
Composite
5 µm
5 µm

Fig 1

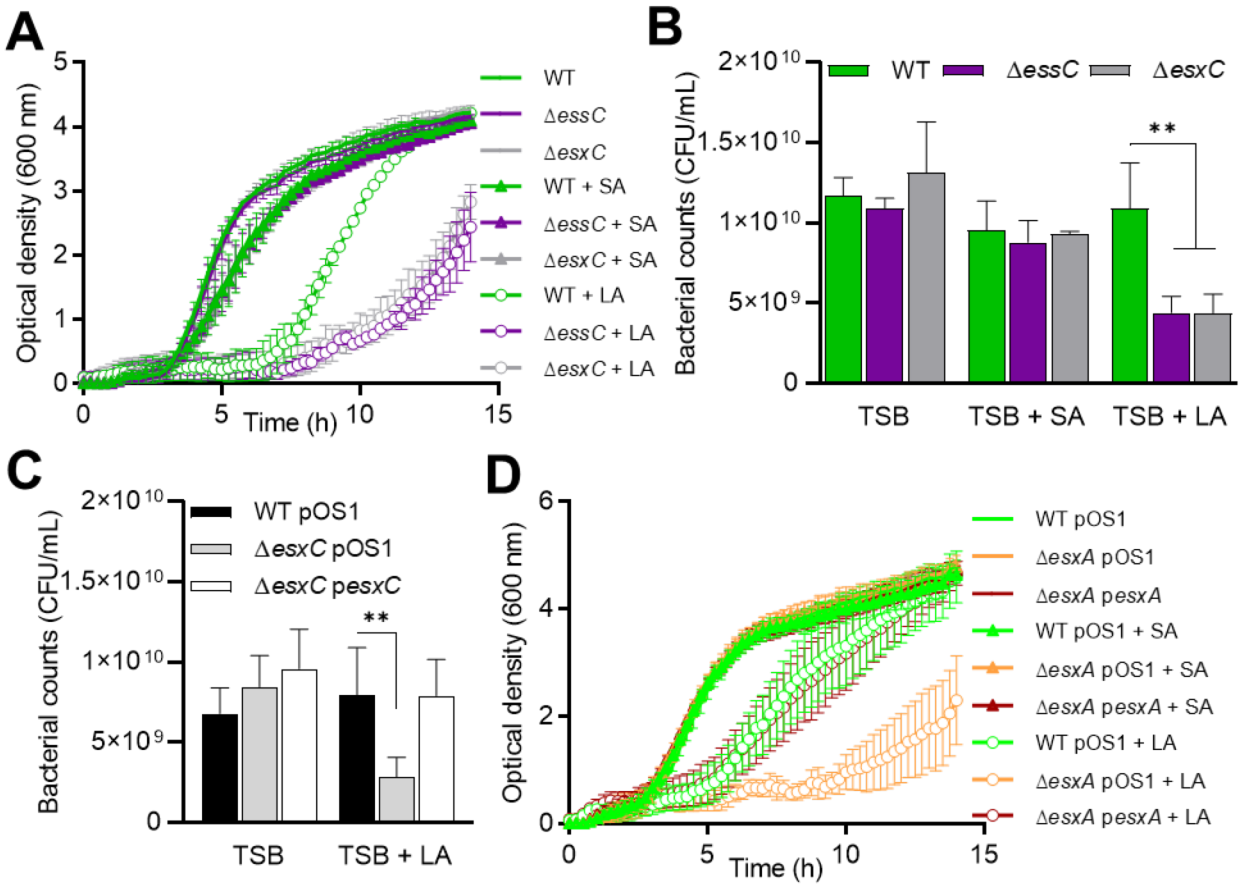
A
Optical density (600 nm)
Time (h)
WT
ΔessC
ΔesxC
WT + SA
ΔessC + SA
ΔesxC + SA
WT + LA
ΔessC + LA
ΔesxC + LA
B
Bacterial counts (CFU/mL)
WT
ΔessC
ΔesxC
**
TSB
TSB + SA
TSB + LA
C
Bacterial counts (CFU/mL)
WT pOS1
ΔesxC pOS1
ΔesxC pesxC
**
TSB
TSB + LA
D
Optical density (600 nm)
Time (h)
WT pOS1
ΔesxA pOS1
ΔesxA pesxA
WT pOS1 + SA
ΔesxA pOS1 + SA
ΔesxA pesxA + SA
WT pOS1 + LA
ΔesxA pOS1 + LA
ΔesxA pesxA + LA

Fig 2

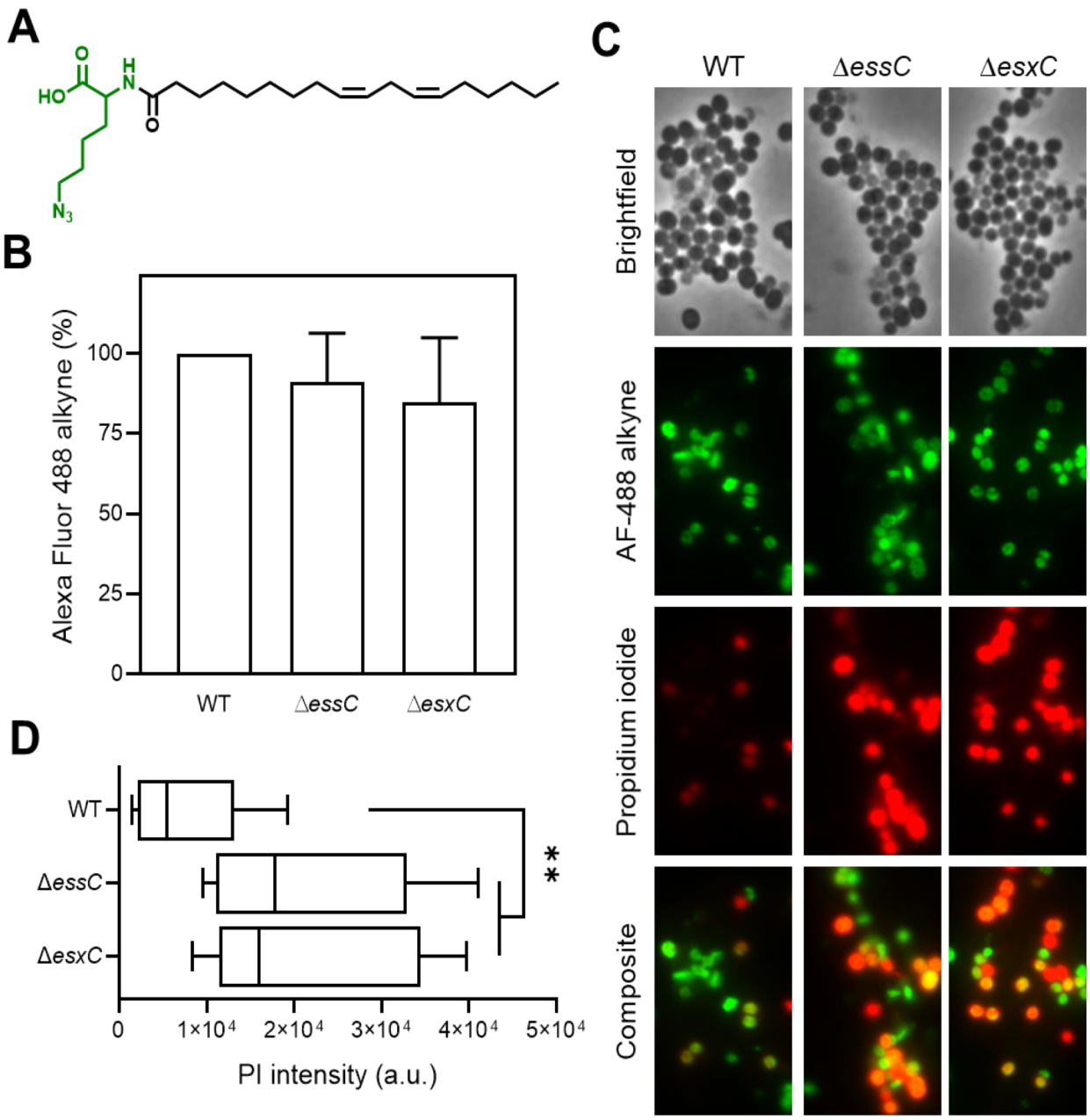
A
HO
O
H
N
O
N_3
B
Alexa Fluor 488 alkyne (%)
100
75
50
25
0
WT
ΔessC
ΔesxC
C
WT
ΔessC
ΔesxC
Brightfield
AF-488 alkyne
Propidium iodide
Composite
D
WT
ΔessC
ΔesxC
**
0
1×10⁴
2×10⁴
3×10⁴
4×10⁴
5×10⁴
PI intensity (a.u.)

Fig 3

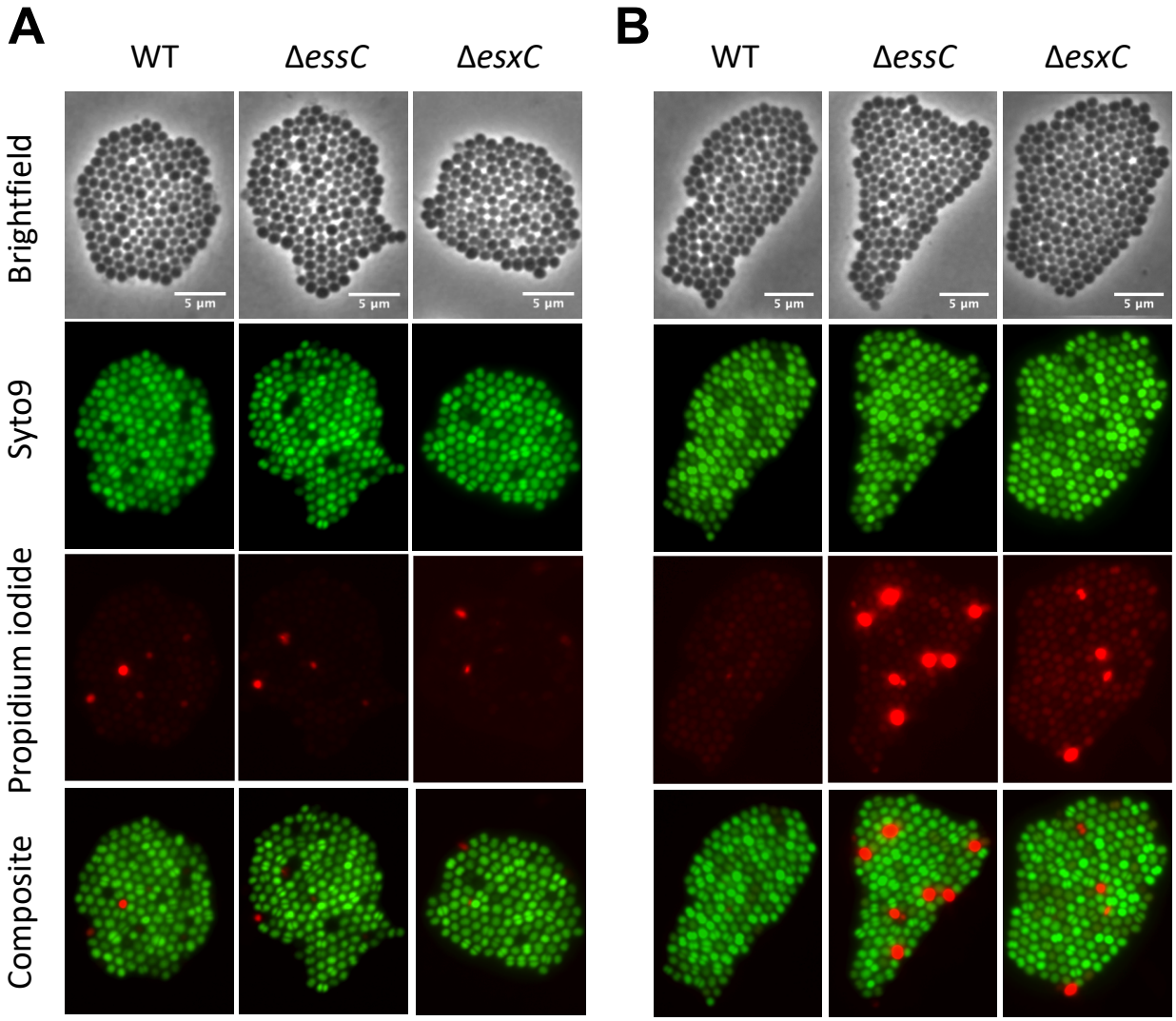
A
WT
ΔessC
ΔesxC
Brightfield
Syto9
Propidium iodide
Composite
5 µm
B
WT
ΔessC
ΔesxC
5 µm
C
WT
ΔesxC
ΔessC
SYTO 9 / PI fluorescence
10
8
6
4
2
0
**
***
***
TSB
TSB + LA

Fig 4

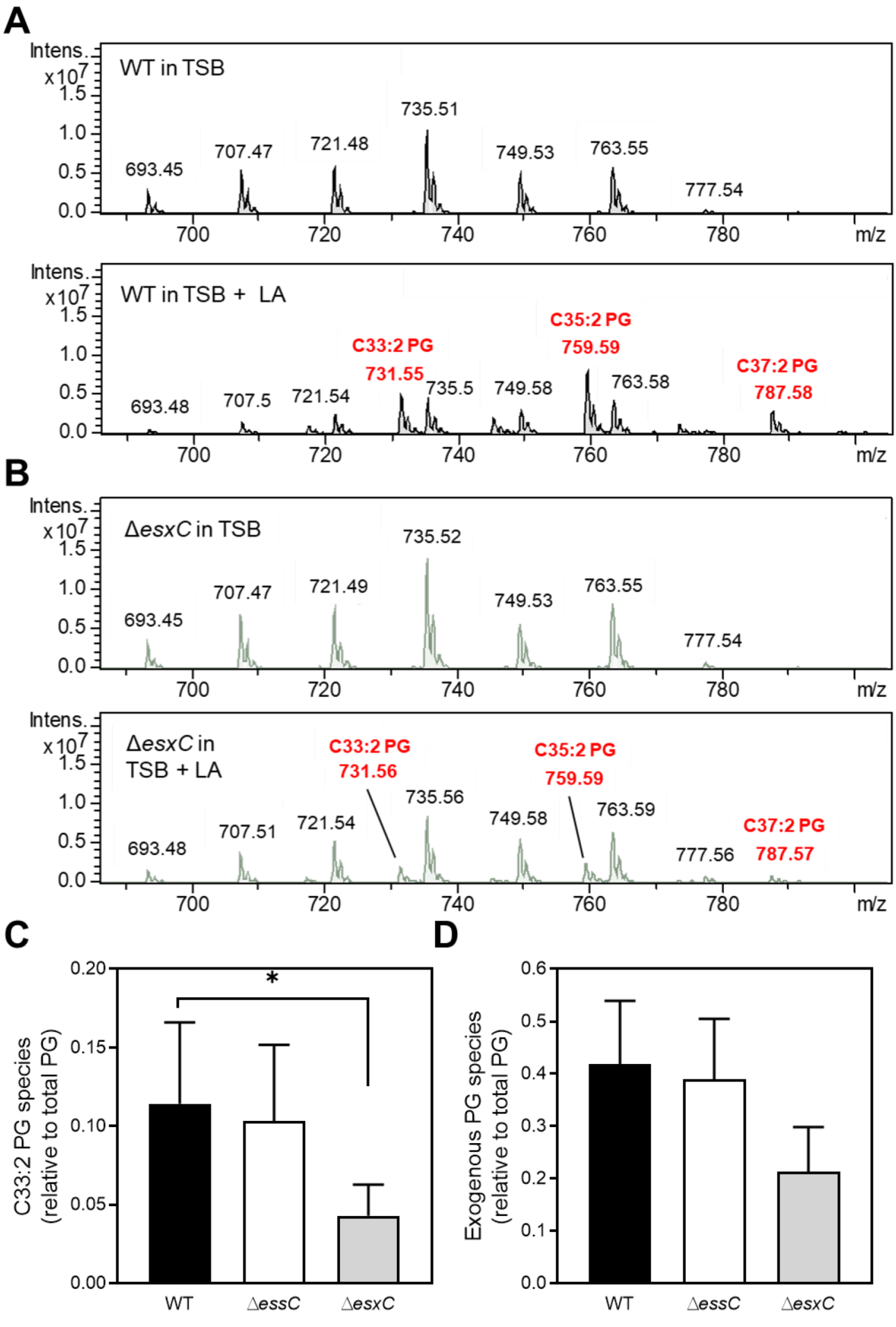
A
Intens.
x10^7
WT in TSB
693.45
707.47
721.48
735.51
749.53
763.55
777.54
m/z
WT in TSB + LA
C33:2 PG
731.55
C35:2 PG
759.59
C37:2 PG
787.58
693.48
707.5
721.54
735.5
749.58
763.58
B
ΔesxC in TSB
735.52
707.47
721.49
749.53
763.55
693.45
777.54
ΔesxC in
TSB + LA
C33:2 PG
731.56
C35:2 PG
759.59
735.56
749.58
763.59
707.51
721.54
693.48
777.56
C37:2 PG
787.57
C
C33:2 PG species
(relative to total PG)
*
WT
ΔessC
ΔesxC
D
Exogenous PG species
(relative to total PG)
WT
ΔessC
ΔesxC

Fig 5

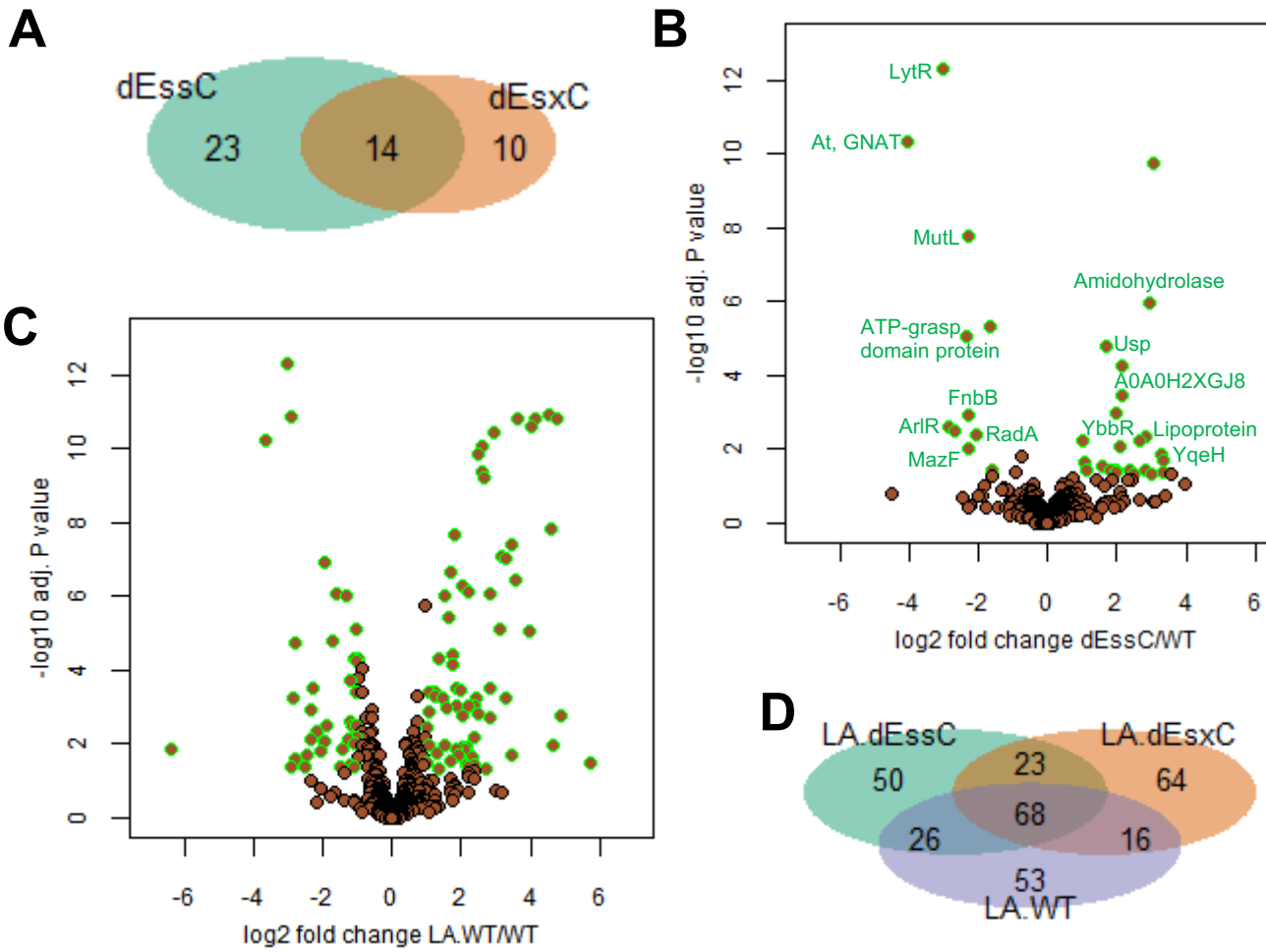
A
dEssC
dEsxC
23
14
10
B
LytR
At, GNAT
MutL
Amidohydrolase
ATP-grasp
domain protein
Usp
A0A0H2XGJ8
FnbB
ArlR
RadA
YbbR
Lipoprotein
MazF
YqeH
-log10 adj. P value
log2 fold change dEssC/WT
C
-log10 adj. P value
log2 fold change LA.WT/WT
D
LA.dEssC
LA.dEsxC
LA.WT
50
23
64
68
26
16
53

Fig 6

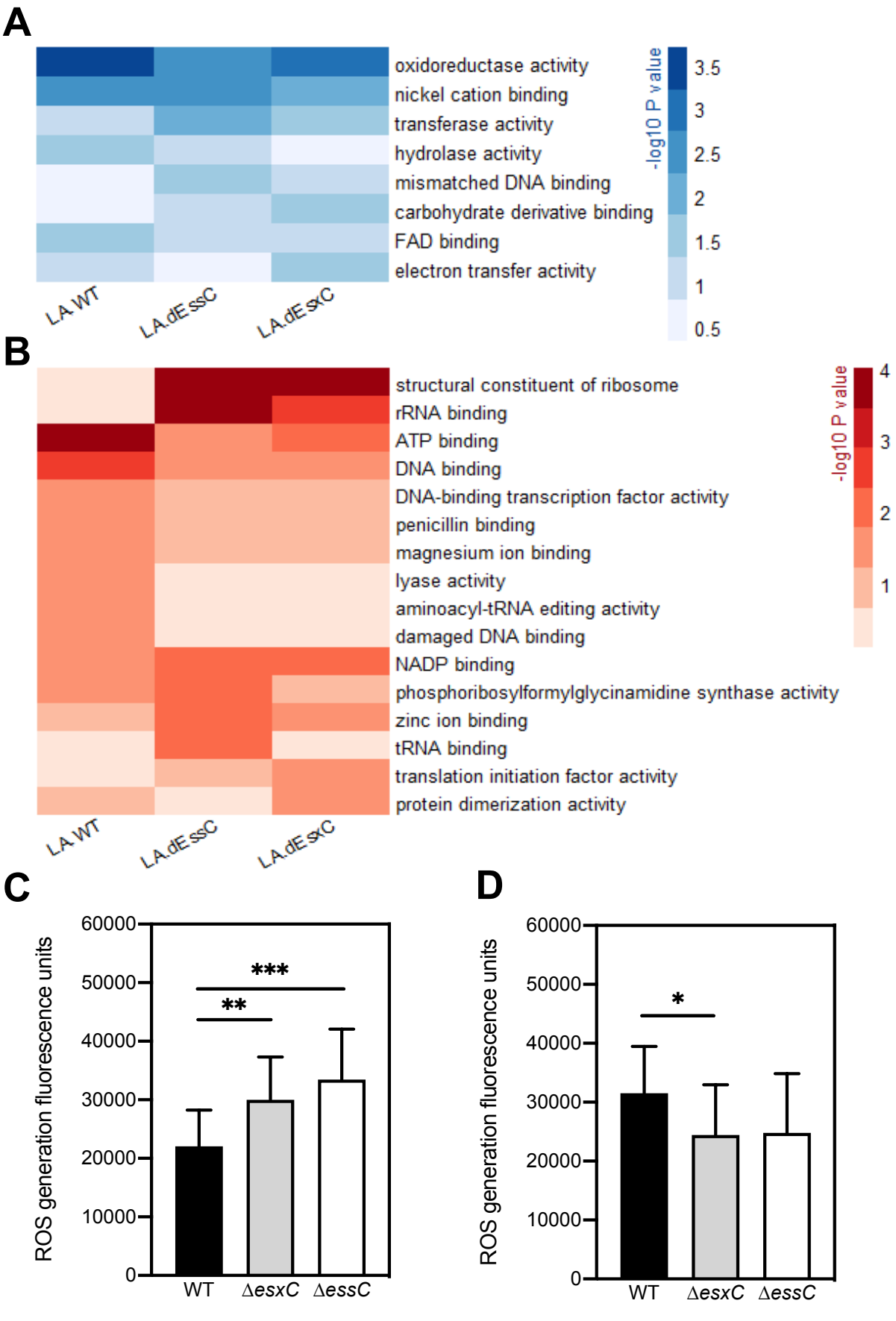
A
oxidoreductase activity
nickel cation binding
transferase activity
hydrolase activity
mismatched DNA binding
carbohydrate derivative binding
FAD binding
electron transfer activity
-log10 P value
3.5
3
2.5
2
1.5
1
0.5
LA.WT
LA.dEssC
LA.dEsxC
B
structural constituent of ribosome
rRNA binding
ATP binding
DNA binding
DNA-binding transcription factor activity
penicillin binding
magnesium ion binding
lyase activity
aminoacyl-tRNA editing activity
damaged DNA binding
NADP binding
phosphoribosylformylglycinamidine synthase activity
zinc ion binding
tRNA binding
translation initiation factor activity
protein dimerization activity
-log10 P value
4
3
2
1
LA.WT
LA.dEssC
LA.dEsxC
C
ROS generation fluorescence units
60000
50000
40000
30000
20000
10000
0
***
**
WT
ΔesxC
ΔessC
D
ROS generation fluorescence units
60000
50000
40000
30000
20000
10000
0
*
WT
ΔesxC
ΔessC

Fig 7